JACS
JOURNAL OF THE AMERICAN CHEMICAL SOCIETY
Article
pubs.acs.org/JACS

Catalytic Mechanisms of Direct Pyrrole Synthesis via Dehydrogenative Coupling Mediated by PNP-Ir or PNN-Ru Pincer Complexes: Crucial Role of Proton-Transfer Shuttles in the PNP-Ir System

Shuanglin Qu,[‡] Yanfeng Dang,[‡] Chunyu Song,[‡] Mingwei Wen,[‡] Kuo-Wei Huang,[§] and Zhi-Xiang Wang*[,‡,∥]

[‡]School of Chemistry and Chemical Engineering, University of the Chinese Academy of Sciences, Beijing, 100049, China
[§]KAUST Catalysis Center and Division of Physical Science and Engineering, King Abdullah University of Science and Technology, Thuwal 23955-6900, Kingdom of Saudi Arabia
[∥]Collaborative Innovation Center of Chemical Science and Engineering, Tianjin, 300072, China

Supporting Information

ABSTRACT: Kempe et al. and Milstein et al. have recently advanced the dehydrogenative coupling methodology to synthesize pyrroles from secondary alcohols (e.g., **3**) and β-amino alcohols (e.g., **4**), using PNP-Ir (**1**) and PNN-Ru (**2**) pincer complexes, respectively. We herein present a DFT study to characterize the catalytic mechanism of these reactions. After precatalyst activation to give active **1A**/**2A**, the transformation proceeds via four stages: **1A**/**2A**-catalyzed alcohol (**3**) dehydrogenation to give ketone (**11**), base-facilitated C−N coupling of **11** and **4** to form an imine-alcohol intermediate (**18**), base-promoted cyclization of **18**, and catalyst regeneration via H_2 release from **1R**/**2R**. For alcohol dehydrogenations, the bifunctional double hydrogen-transfer pathway is more favorable than that via β-hydride elimination. Generally, proton-transfer (H-transfer) shuttles facilitate various H-transfer processes in both systems. Notwithstanding, H-transfer shuttles play a much more crucial role in the PNP-Ir system than in the PNN-Ru system. Without H-transfer shuttles, the key barriers up to 45.9 kcal/mol in PNP-Ir system are too high to be accessible, while the corresponding barriers (<32.0 kcal/mol) in PNN-Ru system are not unreachable. Another significant difference between the two systems is that the addition of alcohol to **1A** giving an alkoxo complex is endergonic by 8.1 kcal/mol, whereas the addition to **2A** is exergonic by 8.9 kcal/mol. The thermodynamic difference could be the main reason for PNP-Ir system requiring lower catalyst loading than the PNN-Ru system. We discuss how the differences are resulted in terms of electronic and geometric structures of the catalysts and how to use the features in catalyst development.

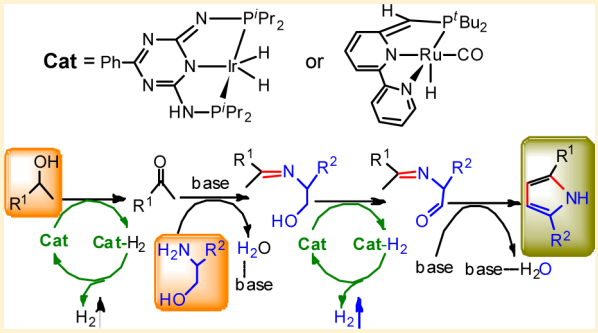

1. INTRODUCTION

Coupling via acceptorless dehydrogenation (AD), known as dehydrogenative coupling, is emerging as a powerful, atom-economic, and environmentally benign synthetic methodology for organic synthesis via C−C, C−N, and C−O couplings.[1−4] The essence of dehydrogenative coupling lies in that the employed catalyst is able to activate a substrate such as alcohol to a more reactive intermediate (i.e., ketone or aldehyde) via dehydrogenation without using additional sacrificial organic hydrogen acceptor or inorganic oxidant, then the reactive intermediate couples with its partners to finally form more stable products. Dehydrogenative coupling has been utilized to synthesize various important chemicals such as amides,[2] imines,[3a] and esters.[4] Continuing these successes, dehydrogenative coupling has recently found application in pyrrole synthesis.[5−9] Pyrroles are key building units in many drugs[10] and biologically active molecules[11] and also have applications in conducting polymers[12] and molecular devices of optics[13] and electronics.[14] Routes such as Hantzsch,[15] Knorr,[16] and Paal−Knorr[17] reactions have been developed to synthesize pyrroles, but the drawbacks of these methods (e.g., availability of substrates, multisteps synthetic operations, functional group compatibility, regioselectivity, and harsh conditions) have encouraged chemists to discover more efficient and greener routes to synthesize pyrroles.[18,19] On the basis of the dehydrogenative coupling methodology, Crabtree et al. coupled 1,4-diols and amines to produce pyrroles using ruthenium diphosphine diamine complexes as catalyst.[5] Recently, Beller et al. synthesized aryl-substituted pyrroles from aryl ketones, 1,2-diols, and amines by using $[Ru_3(CO)_{12}]$[6] or $[Ru(p\text{-cymene})Cl_2]_2$[7] as catalyst precursors. More recently, as exemplified by

Received: November 19, 2013
Published: March 10, 2014

eq 1, Kempe et al. synthesized pyrroles by coupling secondary alcohols with β-amino alcohols, using the PNP-Ir pincer

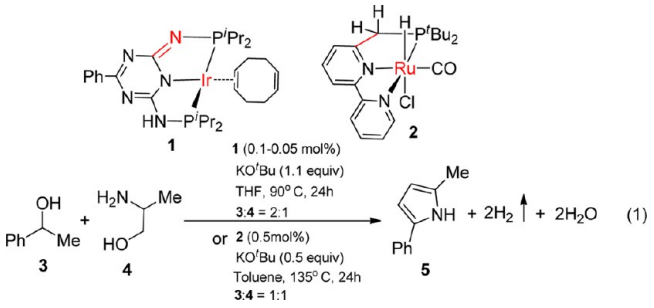

complex **1** as mediator.[8] Soon after, Milstein et al. found that their PNN-Ru pincer complex **2** could also efficiently catalyze pyrrole synthesis from the same/or similar substrates (see eq 1).[9]

The novelty of AD reactions and AD-based couplings has invited computational studies to understand their mechanisms in detail.[20,21] Previously, our group has investigated the mechanisms of AD reactions of secondary alcohol[21a] and reversible hydrogenation/dehydrogenation of nitrogen heterocycles catalyzed by other iridium complexes (**6** and **7**[22] in Scheme 1),[21b] hydrogenation of carbonate giving methanol,[21c]

Scheme 1. Active Transition-Metal Catalysts Involved in the AD Reactions (6 and 7) and Dehydrogenative Couplings for Amide (8) and Imine Synthesis (9) and an *in Silico* Example (10) of Metal-Free Counterparts of 8 and 9

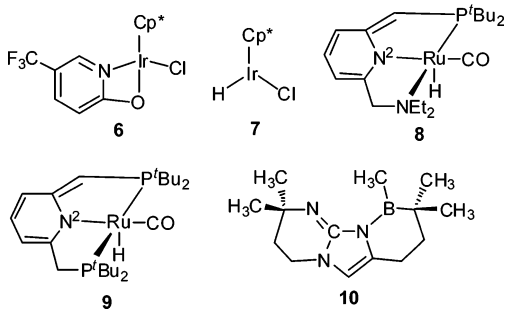

and amide[21d] or imine[21e] synthesis from alcohols and amines, catalyzed by PNN-Ru (**8**)[2a,d] or PNP-Ru (**9**)[3] pincer complexes. Furthermore, by mimicking the mechanism of H_2 activation by **8** and **9**, we computationally designed their metal-free counterparts (e.g., **10**).[23] The energetic results indicated these *in silico* molecules could activate H_2[23b] and NH_3[23c] nearly reversibly. In this context, we were intrigued by the catalytic pyrrole synthesis via dehydrogenative coupling.[8,9] Different from amide and imine productions that only involve C−N bond formation, pyrrole synthesis via eq 1 involves selective C−N and C−C coupling events. For the alcohol AD step involved in the amide or imine synthesis from alcohols and amines, catalyzed by **8** and **9**, we have computationally shown that the bifunctional double hydrogen transfer (BDHT) dehydrogenation pathway via metal−ligand cooperation could be more favorable than the previously proposed β-H elimination pathway.[21d,e] Our computational results have recently been supported by another computational study reported by Lee and co-workers.[20v] Experimentally, Milstein and co-workers also concluded that β-H elimination pathway catalyzed by **9** is unlikely.[24] It is unclear whether this is the case for the alcohol dehydrogenation catalyzed by the activated PNP-Ir complex (i.e., **1A** in Scheme 2). Both **1** and **2** could promote the reaction, but their activated species have different active sites (=N···Ir in **1A** vs =CH···Ru in **2A**, see Scheme 2 below). It is intriguing to know how they act similarly or differently. Regarding to the BDHT mechanism, it is noteworthy that in the reduction of CO_2 with H_2 mediated by the analogs of **1R**/**2R** in Scheme 2,[25−28] the reaction step of CO_2 with these hydride analogs does not take place to produce formic acid via a BDHT hydrogenation process, instead CO_2 inserts into metal-H bond.[27,29] In addition, the amide[2a,21d] or imine[3,21e] synthesis from alcohols and amines, catalyzed by PNN-Ru (**8**) or PNP-Ru (**9**), respectively, needed no base, but base was indispensable for the pyrrole synthesis (see eq 1). It is interesting to understand the role of the base. Herein we present a computational study on the catalytic mechanism of the pyrrole synthesis described by eq 1 and compare the behaviors of the two catalysts. An in-depth mechanistic understanding in terms of energetics and structures could help improve the current catalytic systems or developing new catalysts.

2. COMPUTATIONAL DETAILS

For a catalytic system, both geometric and electronic structures of catalyst and substrates have profound influences on both catalytic mechanism and efficiency, thus we used actual compounds rather than simplified models in this study. All structures were optimized in the gas phase at M06[30]/BSI level, where BSI represents a basis set with 6-31G(d,p)[31] for nonmetal atoms and SDD[32] for Ru and Ir. Harmonic frequency analysis calculations were subsequently performed to verify the optimized geometries to be minima (no imaginary frequency) or transition states (TSs, having unique one imaginary frequency). The energies were then improved by M06/BSII//M06/BSI single-point calculations with solvent effects accounted by the SMD[33] solvent model, using the experimental solvent (THF). BSII denotes a basis set with 6-311++G(d,p)[34] for nonmetal atoms and SDD for Ru and Ir. The refined energies were then corrected to enthalpies and free energies at 298.15 K and 1 atm, using the gas-phase M06/BSI harmonic frequencies. It should be emphasized that such thermal corrections based on the ideal gas phase model inevitably overestimate entropy contributions to free energies for reactions in solvent, in particular for reactions involving multicomponent change, because of ignoring the suppressing effect of solvent on the rotational and transitional freedoms of substrates. Since no standard quantum mechanics-based approach is available to accurately calculate entropy in solution, we adopted the approximate approach proposed by Martin et al.[35] According to their approach, a correction of 4.3 kcal/mol applies to per component change for a reaction at 298.15 K and 1 atm (i.e., a reaction from *m*- to *n*-components has an additional correction of $(n - m) \times 4.3$ kcal/mol). In agreement with this approach, Holm and Rybak-Akimova found a 4−5 kcal/mol overestimation of entropic contribution by comparing the experimental and computed values.[36] Yu and co-workers showed that the ideal gas-phase based corrections could overestimate the entropy contributions by 50−60% in their 2-to-1 reactions.[37] As shown by eq 1, the present transformation involves multicomponent change; the overall transformation is from two components (**3** + **4**) to five components (**5** + 2H_2O + 2H_2), thus the entropy overestimations must be taken into account. Previously, we applied the correction protocol for mechanistic studies of various catalytic reactions and found such corrected free energies were more reasonable than enthalpies and uncorrected free energies.[21b,c,38] In the following, we discuss the mechanism in terms of the corrected free energies and give the enthalpies for references in the brackets in the relevant figures. All calculations were carried out using Gaussian 09 program.[39] Total energies and Cartesian coordinates of all optimized structures are given in Supporting Information.

dx.doi.org/10.1021/ja411568a | J. Am. Chem. Soc. 2014, 136, 4974−4991

Scheme 2. Schematic Illustration of the Whole Catalytic Cycle for the Production of 5 from 1-Phenol Ethanol (3) and 2-Amino-1-butanol (4), Catalyzed by 1A or 2A

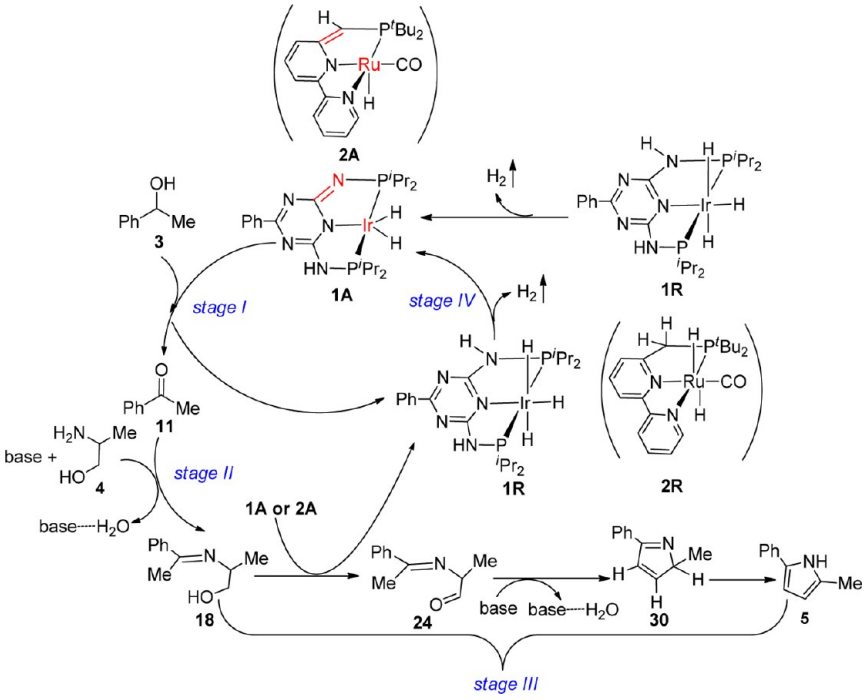

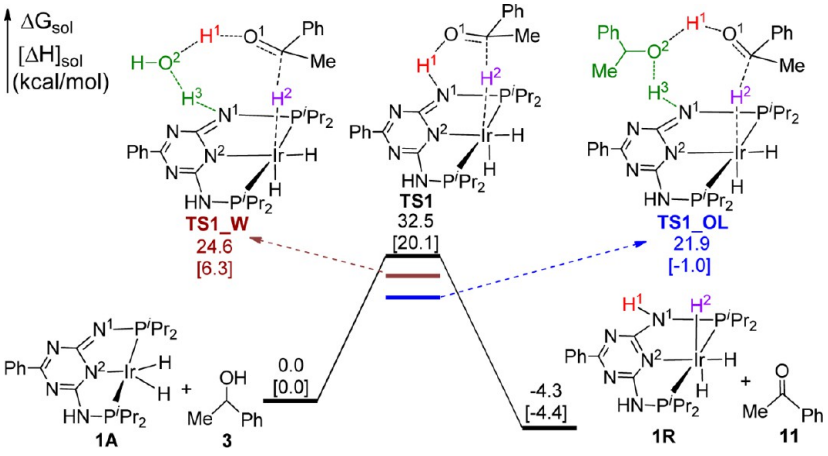

Figure 1. BDHT pathway for **1A**-catalyzed dehydrogenation of **3**, along with the relative free energies and enthalpies (in brackets).

3. RESULTS AND DISCUSSIONS

The transition-metal complexes PNP-Ir (**1**) and PNN-Ru (**2**) were applied to synthesize various pyrroles catalytically. We chose eq 1 reaction for our mechanistic investigation. Both **1** and **2** could mediate the same transformation, but they are catalyst precursors rather than actual catalysts. Experimentally, Kempe et al. identified a PNP-Ir(III) trihydride (**1R** in Scheme 2) to be the resting state and obtained its crystal structure under catalytic conditions. Because in **1R** the $-NH-P^iPr_2$ arm is saturated and the Ir(III) center is saturated both coordinatively and electronically (i.e., an 18*e* Ir(III) complex), **1R** needs to be activated by releasing H_2. As will be discussed, there are two possible H_2-elimination pathways leading **1R** to the active catalyst **1A** (a PNP-Ir(III) dihydride). The PNN-Ru complex **2** can be activated by a base[40] to the active species **2A** (a PNN-Ru(II) monohydride) which was also examined to be able to carry out the reaction alone. On the basis of experimental results, reaction sequence proposed by Kempe et al. and Milstein et al., and our computational results, Scheme 2 sketches the whole catalytic cycle for the transformation. After precatalyst activation giving **1A**/**2A**, the catalytic formation of pyrrole proceeds via four stages, namely, stage I: **1A**/**2A**-catalyzed alcohol dehydrogenation which activates **3** (1-phenol ethanol) to more reactive ketone (**11**); stage II: base-aided C−N bond formation by coupling **11** with *β*-amino alcohol **4** (2-amino-1-butanol) to form an imine-alcohol intermediate (**18**) via dehydration; stage III: intramolecular cyclization of **18** via three substeps including **1A**/**2A**-catalyzed dehydrogenation of the alcohol part of **18**, giving the imine-aldehyde intermediate **24**, base-promoted C−C coupling via dehydration to give the cyclic **30**, and 1,2-H transfer to finally deliver pyrrole (**5**); and stage IV, catalyst recovery by releasing H_2 gas from the resting state (**1R**/**2R**) to regenerate the active species (**1A**/**2A**). In the following, we discuss our computational results in terms of the four stages, using **1A**-catalyzed

dx.doi.org/10.1021/ja411568a | J. Am. Chem. Soc. 2014, 136, 4974−4991

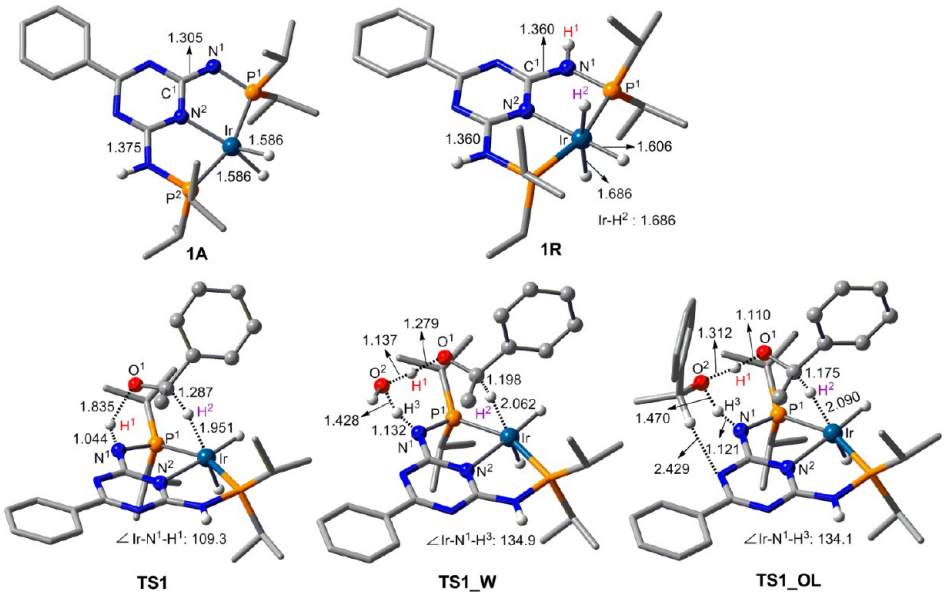

Figure 2. Optimized geometries of key stationary points labeled in Figure 1. Key bond lengths and angles are given in angstroms and degrees, respectively. Trivial H atoms are omitted for clarity.

transformation as a representative in Section 3.1 and then compare the similarities and differences between the two systems in Section 3.2.

3.1. Catalytic mechanism of 1A-system. *3.1.1. Alcohol Dehydrogenation (Stage I).* AD is a crucial step to initiate dehydrogenative coupling reactions, transforming alcohol to more reactive intermediate (ketone or aldehyde). Among the two available alcohols (**3** and **4**), **3** should undergo dehydrogenation preferentially, because **3** is a secondary alcohol while **4** is primary, which was also confirmed by computations (*vide infra*).

The dehydrogenation of alcohol **3** can follow two possible mechanisms, including β-H elimination (inner sphere) and BDHT (outer sphere) mechanisms. In the previous mechanistic studies[20v,21d] of amide formation from alcohol and amine, catalyzed by **8**, the energetic results showed that the BDHT mechanism is more favorable than the β-H elimination one. To examine whether this holds true for the **1A**-catalyzed alcohol dehydrogenation, both BDHT and β-H elimination pathways were considered below.

Figure 1 shows the energy profile for following the BDHT mechanism, and Figure 2 displays the optimized structures of key stationary points labeled in Figure 1. **TS1** illustrates the BDHT mechanism to concertedly transfer the two hydrogen atoms (H^1 and H^2) of **3** to the metal−ligand bifunctional active site composed of the Lewis acidic Ir(III) center and the Lewis basic sp^2 N center of the $=N-P^iPr_2$ arm (hereafter, we symbolize the bifunctional active site as $=N\cdots Ir$). As the dehydrogenation proceeds to give ketone **11**, the *s*-triazine-based ligand ring becomes aromatic *s*-triazine in **1R**, which provides an aromatization driving force for the dehydrogenation. Note that the aromatization driving force also acts in the alcohol dehydrogenation catalyzed by **6**.[21b] In contrast to the concerted pathway, previous studies showed that the alcohol dehydrogenations mediated by **8** and **9** undergo stepwise pathways.[21d,e] We attempted to locate a similar pathway, but geometric optimizations to locate relevant TSs repeatedly converged to **TS1**. This is reasonable; because the previously computed stepwise pathways have very low barriers (1.8 and 0.2 kcal/mol, respectively) for the second hydrogen transfer, those stepwise pathways can approximately be considered as concerted. On the other hand, the different DFT functionals, active sites, and substrates could be other factors for the difference. Relative to **3** + **1A**, the dehydrogenation barrier (**TS1**) is 32.5 kcal/mol. The high barrier is manifested by the overstretched breaking O^1-H^1 bond (1.835 Å) in its structure (Figure 2). A barrier of 32.5 kcal/mol could be high for the dehydrogenation, thus we envisioned a proton/hydrogen-transfer (H-transfer) shuttle might be involved. Previous studies have shown that H-transfer shuttles could facilitate H-transfer process greatly.[20l,21c,41] Most recently, in the study of CO_2 reduction mediated by pyridine (Py) in the electrocatalytic Py/p-GaP system in aqueous, Musgrave et al.[42] showed that, for the proton transfer step from PyH^0 + CO_2 to $PyCOOH^0$, the computed barrier (45.7 kcal/mol at MP2 level) via direct transfer is much higher than the experimental value (~16.5 kcal/mol), but after using H-transfer shuttles composed of up to three water molecules, the computed values (13.6−16.5 kcal/mol) are in good agreement with the experimental value. In the present system, either alcohol (one of the substrates) or water (one of the side products) can serve as H-transfer shuttles. When a water molecule is used as the shuttle (see **TS1_W**), the barrier is reduced significantly by 7.9 kcal/mol (to 24.6 kcal/mol). In agreement with our previous finding[41a] that alcohol is more effective than water in mediating H-transfer, when using alcohol **3** as the shuttle, the barrier (**TS1_OL**) is further dropped to 21.9 kcal/mol. The use of **3** rather than **4** to construct H-transfer is due to that the secondary alcohol **3** is more effective than the primary alcohol **4** (see Figure S11). Comparing **TS1_W** and **TS1_OL** with **TS1** (Figure 2), it can be observed that, as reflected by the larger $\angle IrN^1H^3$ angles (134.9° in **TS1_W** and 134.1° in **TS1_OL**) than the corresponding $\angle IrN^1H^1$ (109.3°) in **TS1**, the transferring H interacts with the lone pair of N^1 geometrically more suitable in the former two TSs than in the later (see Section 3.2 for more details). Consequently, the distances of forming and breaking bonds in the **TS1_W** and **TS1_OL** are now in the more reasonable range. The geometric comparisons

dx.doi.org/10.1021/ja411568a | J. Am. Chem. Soc. 2014, 136, 4974−4991

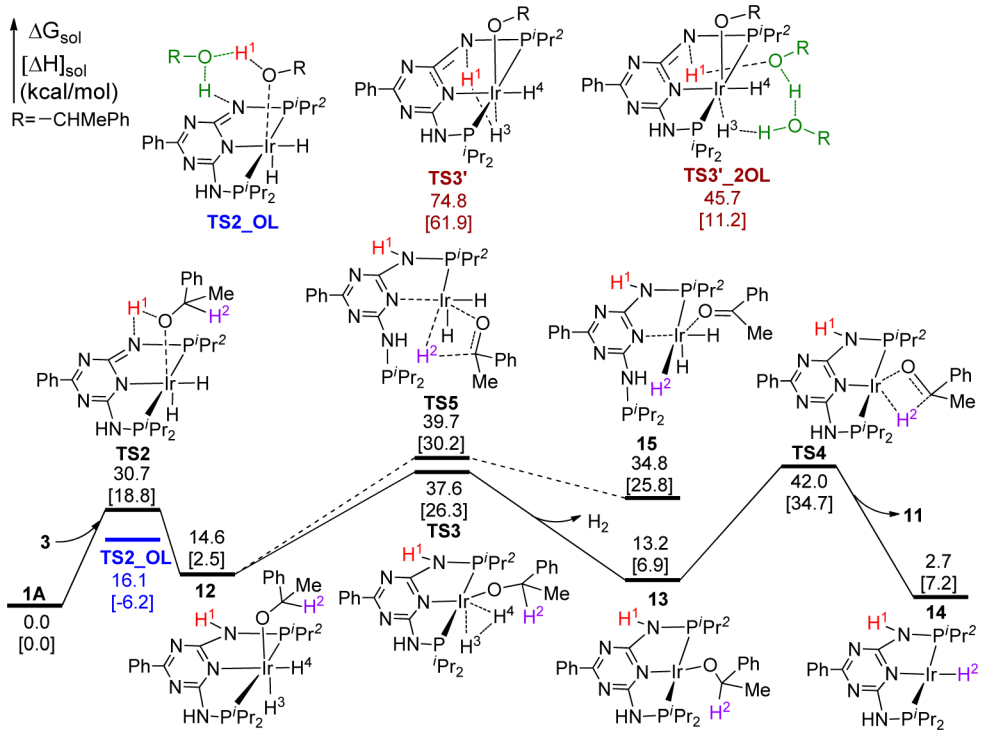

Figure 3. β-H elimination pathway for the **1A**-catalyzed dehydrogenation of **3**, along with the relative free energies and enthalpies (in brackets).

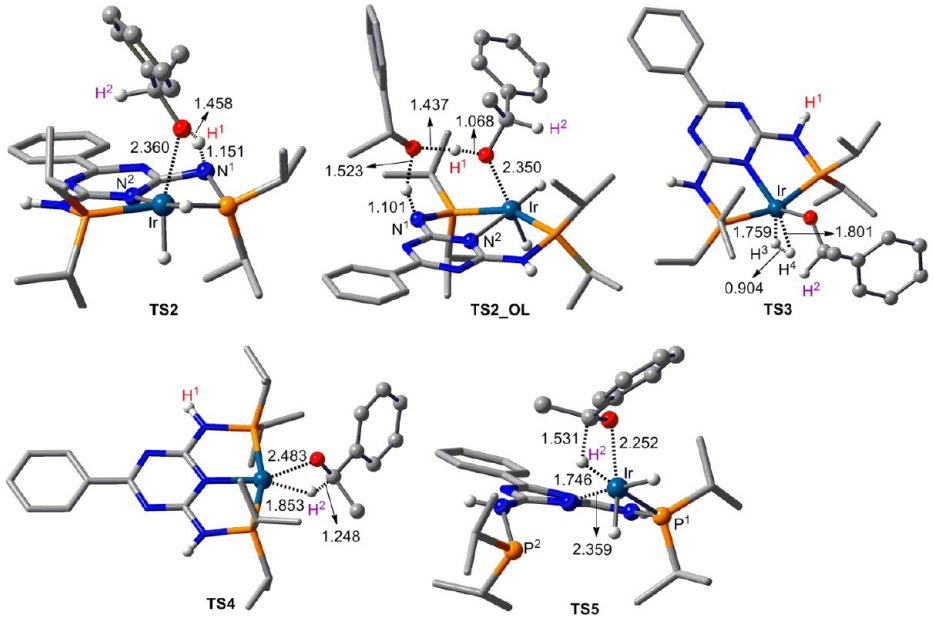

Figure 4. Optimized structures of the key stationary points labeled in Figure 3. Key bond lengths are given in angstroms, and trivial H atoms are omitted for clarity.

elucidate why these shuttles can facilitate the BDHT dehydrogenation pathway significantly. The BDHT dehydrogenation transfers both positively charged H^1 and H^2 of **3** to a proton and a hydride in **1R**, resulting in ketone C═O bond. Oppositely, the protonic and hydridic hydrogen atoms in BH_3NH_3 can feasibly transfer to the C═O bond of CO_2, bearing positive charges.[43]

Figure 3 displays the energy profile for following the β-H elimination mechanism and the optimized structures of the key stationary points labeled in Figure 3 are shown in Figure 4. In this mechanism, the O−H bond of **3** first breaks on the ═N··· Ir active site via **TS2** with a barrier of 30.7 kcal/mol, giving the aromatized Ir complex **12**. Similar to the **3** dehydrogenation via BDHT mechanism, the barrier can also be lowered by using an alcohol H-transfer shuttle (see **TS2_OL**). After breaking the O−H bond, the β-H elimination can proceed via two different pathways. Along the solid pathway, the two *cis* hydrides in **12** undergoes reductive elimination to form H_2 via **TS3**, leading to the reduced 16*e* Ir(I) complex **13**. The complex **13** now has a vacant site for β-H elimination taking place via **TS4**, resulting in ketone **11** and an 16*e* PNP-Ir(I) complex **14**. Alternatively, the β-H elimination (the dashed pathway) can take place from **12**

dx.doi.org/10.1021/ja411568a | J. Am. Chem. Soc. 2014, 136, 4974−4991

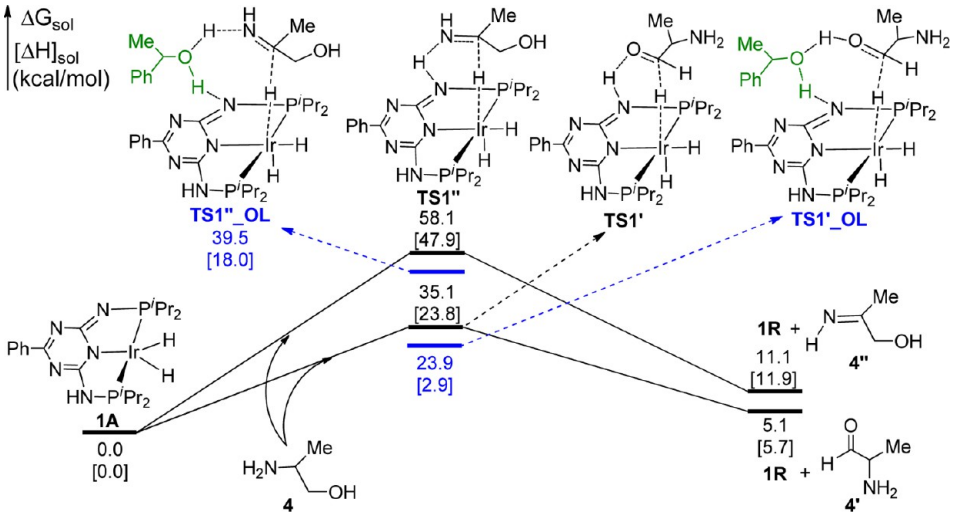

Figure 5. Free energy profile for **1A**-catalyzed dehydrogenations of amine and alcohol parts of **4**, along with enthalpies (in brackets). Optimized geometries of transition states see Figure S6.

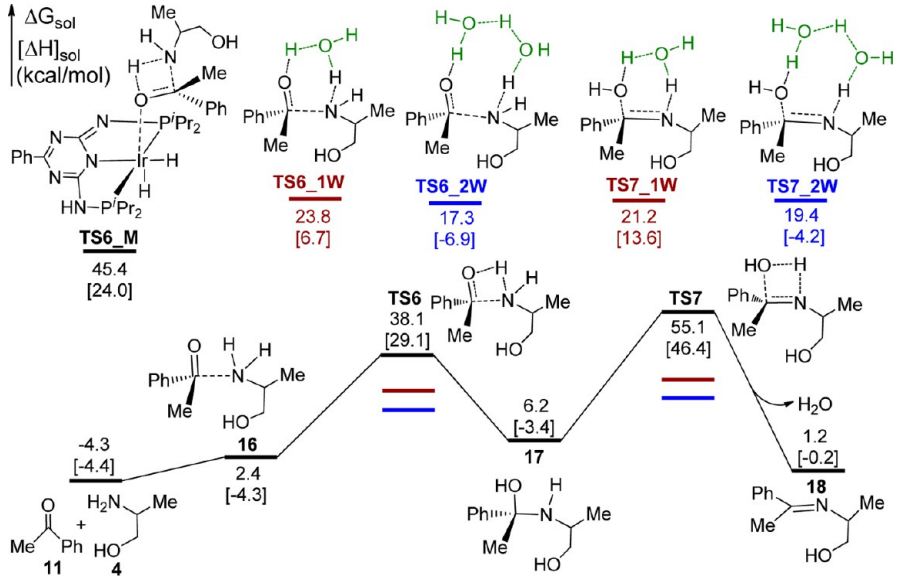

Figure 6. Pathway for the C−N coupling of **11** and **4** under neutral condition, leading **11** + **4** to **18** + H_2O, along with the relative free energies and enthalpies (in brackets). Optimized geometries of key stationary points see Figure S7.

via **TS5**. In **TS5**, one of the arms is dissociated, allowing the Ir center to have a vacant site for β-H elimination. From **TS5**, an intermediate **15** can be resulted. By closing the dissociated arm ligand, ketone **11** dissociates to give the resting state (**1R**). Because of the high relative energies of **TS5** and **15**, we did not pursue the details leading **15** to **11** + **1R**. From **1A**+ **3** to **TS5**, there is a third possible channel, which was considered in a previous study of amide synthesis catalyzed by **8**.[20w] Applying the pathway to the present case, the −NH-P^{i}Pr$_2$ arm first opens, followed by the coordination of **3** to the Ir center, and then the proton on the OH group transfers to the N center of the ═N−P^{i}Pr$_2$ arm. Because this channel also needs to pass the high **TS5**, we excluded the possibility without characterizing details. Finally, we examined the possibility of H_2 release from **12** by eliminating the protonic H^1 and hydridic H^3. However, the barrier is very high (74.8 kcal/mol relative to **1A** + **3**, see **TS3′** in Figure 3) and remains to be as high as 45.7 kcal/mol even after using a shuttle of **3** dimer (see **TS3′_2OL**), excluding the possibility.

For the **1A**-catalyzed alcohol dehydrogenation via β-H elimination (Figure 3), the overall barrier is 42.0 kcal/mol (**TS4**) or 39.7 kcal/mol (**TS5**), which is significantly higher than the 21.9 kcal/mol (**TS1_OL** with an H-transfer (**3**) shuttle) and is also higher than the 32.5 kcal/mol (**TS1** without using any H-transfer shuttle). Moreover, the intermediate (**14**) resulted from β-H elimination (the solid pathway in Figure 3) is a PNP-Ir(I) complex which has a barrier of 40.2 kcal/mol for the dehydrogenation of alcohol **3** (see details in stage IV). The high dehydrogenation barrier is also in disagreement with the experimental fact that these transformations are catalytic, and we thus did not further examine the details. The energetic comparisons indicate that the BDHT mechanism is also more favorable than β-H elimination for the **1A**-catalyzed alcohol dehydrogenation. Owing to the overwhelming preference of BDHT over the β-H elimination, we only considered the BDHT mechanism for the following dehydrogenation processes.

dx.doi.org/10.1021/ja411568a | J. Am. Chem. Soc. 2014, 136, 4974−4991

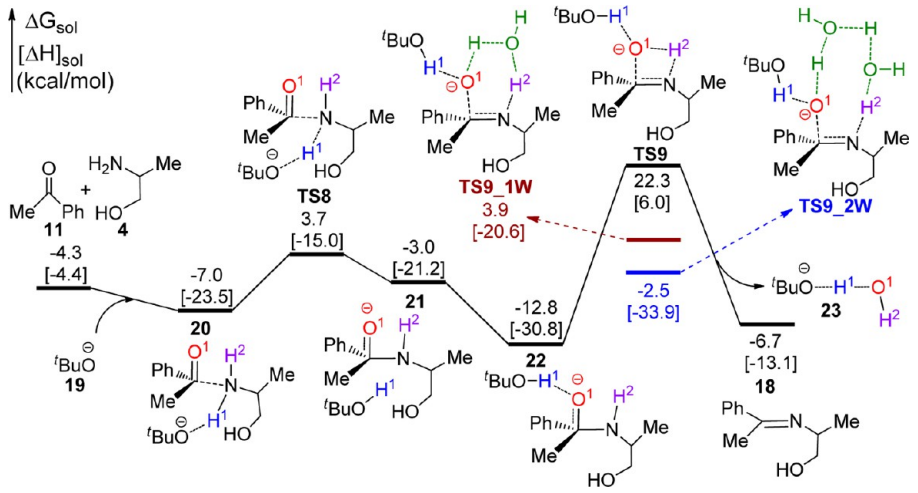

Figure 7. Pathway for the C−N coupling of **11** with **4** catalyzed by the base (^{t}BuO$^-$), leading to **18** + **23**, along with the relative free energies and enthalpies (in brackets). Optimized geometries of key stationary points see Figure S8.

In addition to alcohol **3**, the β-amino alcohol **4** also presents in the system, which may compete with **3** for dehydrogenation. In principle, as proposed by Kempe et al.,[8] if **4** dehydrogenates first, the resultant aldehyde intermediate could also react with **3** via β-alkylation, finally leading to pyrrole **5** (see Figure S6 in ref 8). We examined the dehydrogenations of amine and alcohol parts of **4**, as shown in Figure 5. When using alcohol **3** as an H-transfer shuttle, the dehydrogenation barriers for alcohol and amine parts are 23.9 and 39.5 kcal/mol, respectively, which are higher than the 21.9 kcal/mol barrier for the dehydrogenation of **3**. Moreover, these dehydrogenations of **4** are thermodynamically less favorable than that of **3**; the dehydrogenation of **3** is exergonic by 4.3 kcal/mol, while the dehydrogenations of **4** are endergonic by 5.1 (alcohol part) and 11.1 kcal/mol (amine part), respectively. Because the dehydrogenation of **3** is both kinetically and thermodynamically more favorable than those of **4**, the transformation would preferentially proceed via dehydrogenating **3** first, followed by the next C−N coupling stage (*vide infra*).

3.1.2. Imine Formation (Stage II). The dehydrogenation of **3** in stage I results in reactive ketone (**11**). The next stage is to couple **11** with the β-amino alcohol (**4**), forming a new C−N bond. The coupling mechanism of ketones/aldehydes with amines under neutral condition or under catalysis of an acid catalyst has been studied computationally.[41b,44] Interestingly, Milstein et al. observed that without adding bases such as KO^{t}Bu, the reaction stopped after the dehydrogenation of **3** (stage I).[9] To our knowledge, how a base facilitates coupling of ketones with amines has not been computationally studied. Herein, we examined the coupling mechanisms under neutral condition (denoted as the neutral mechanism hereafter) and under the catalysis of a base catalyst (called the basic mechanism hereafter), aiming to examine if the base plays a catalytic role in forming the imine-alcohol intermediate (**18**).

Figure 6 presents the energy profile for coupling **11** and **4** via the neutral mechanism. The coupling occurs via two successive H-transfer processes. First, the nucleophilic attack of **4** to **11** results in an intermediate **16** which then passes a 1,3-H transfer TS (**TS6**), giving a hemiaminal intermediate (**17**). Subsequently, **17** undergoes dehydration by passing another 1,3-H transfer TS (**TS7**), affording an imine-alcohol intermediate **18**. **TS6** and **TS7** are 42.4 and 59.4 kcal/mol higher than **11** + **4**, excluding the direct coupling mechanism. Nevertheless, both 1,3-H transfer processes can be greatly facilitated by H-transfer shuttles. If using one water molecule as a shuttle, as shown by **TS6_1W** and **TS7_1W**, the two barriers can be reduced to 28.1 and 25.5 kcal/mol, respectively, and if using two water molecules as a bridge, the barriers can be further lowered to 21.6 (**TS6_2W**) and 23.7 kcal/mol (**TS7_2W**), respectively. For the formation of **17** from **4** + **11**, we also examined if the participation of **1A** via **TS6_M** could lower the barrier. Understandably, because the coordination of carbonyl oxygen atom of **11** to Ir center reduces the Lewis basicity of the oxygen atom, **TS6_M** is even 7.3 kcal/mol higher than **TS6**, indicating that **1A** is not involved in the coupling of **4** and **11**.

The energy profile for the C−N coupling catalyzed by a base **19** (i.e., ^{t}BuO$^-$) is drawn in Figure 7. As illustrated by the segment from **11** + **4** + **19** to **22** in Figure 7, after forming a ternary substable intermediate (**20**), the ^{t}BuO$^-$ base grabs the protonic H^1 by crossing a barrier of 10.7 kcal/mol (**TS8**), forming **21** with a C−N bond formed and subsequently leading to a 8.5 kcal/mol (relative to **11** + **4** + **19**) more stable intermediate (**22**) featuring a favorable ^{t}BuO−H$^{\delta+}$···O$^{\delta-}$ interaction. The formation of C−N bond enhances the nucleophilicity of O^1, because of which, the remained H^2 can attack the O^1 via a 1,3-H transfer easier. The barrier (35.1 kcal/mol, **TS9** relative to **22**) for the direct 1,3-H transfer is lower than the corresponding 48.9 kcal/mol (**TS7** relative to **17** in Figure 6) in the neutral mechanism. Nevertheless, the barrier from **22** to **TS9** (35.1 kcal/mol) is somewhat high but can be reduced by H-transfer shuttles. For example, when using a H_2O monomer and H_2O dimer as shuttles, the barriers are lowered to 16.7 (**TS9_1W**) and 10.3 kcal/mol (**TS9_2W**), respectively. Because water molecules were used to construct H-transfer shuttles in the two mechanisms (Figure 6 and 7), the two pathways can be compared energetically. The lowest overall barrier for neutral mechanism is 23.7 kcal/mol (**TS7_2W** relative to **11** + **4** + 2H_2O), which is much higher than the 10.3 kcal/mol (the difference between **22** + 2H_2O and **TS9_2W**) in the basic mechanism. Thus the base facilitates the condensation kinetically, playing a catalytic role. On the other hand, relative to **11** + **4**, the neutral pathway is endergonic by 5.5 kcal/mol, while the basic pathway is exergonic by 2.4 kcal/mol, due to the formation of a more stable ^{t}BuO$^-$···HOH complex (**23**). The energetic results explain well the experimental observation that, if no base was added, the reaction stopped after **3** dehydrogen-

dx.doi.org/10.1021/ja411568a | J. Am. Chem. Soc. 2014, 136, 4974−4991

ation, and neither condensation product **18** nor pyrrole **5** could be observed.[9] This is due to that the neutral pathway is endergonic (**18** + H_2O is 5.5 kcal/mol less stable than **11** + **4**, Figure 6), even though the pathway is kinetically feasible to access **18**. If a base is added, the condensation becomes favorable in terms of both kinetics and thermodynamics. It should be pointed out that, under the base condition, **18** could only exist as a transient intermediate, because it can be easily transformed to the more stable products by subsequent steps (*vide infra*).

The dehydrogenation of **4** may compete with the condensation. To produce pyrrole (**5**) efficiently, the C−N coupling must be preferred over the dehydrogenation of **4**. The energetic results show this to be the case. The C−N coupling via the basic mechanism has an overall barrier of 10.3 kcal/mol and is exergonic by 2.4 kcal/mol, while dehydrogenations of amine and alcohol parts of **4** have barriers of 39.5 and 23.9 kcal/mol, respectively, and are endogonic by 11.1 and 5.1 kcal/mol, respectively (Figure 5).

3.1.3. Intramolecular Cyclization (Stage III). Subsequent to forming the imine-alcohol (**18**) in the preceding stage, the cyclization takes place via forming a new C−C bond between C^1 and C^2 (see **18** in Figure 8). To undergo a C−C coupling,

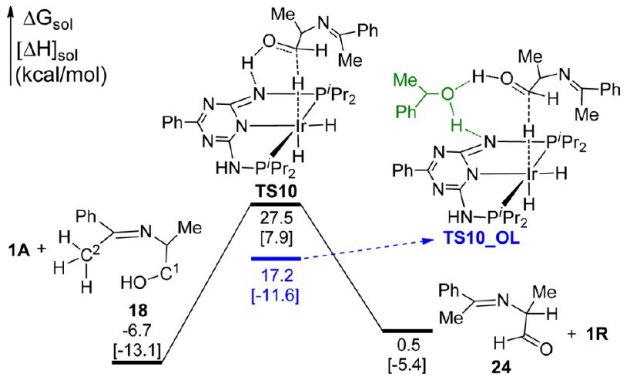

Figure 8. Free energy profile for the dehydrogenation of **18**, leading **18** + **1A** to **24** + **1R**, along with enthalpies (in brackets). Related optimized structures were given in Figure S5.

the alcohol part of **18** needs to be dehydrogenated to the reactive imine-aldehyde intermediate (**24**). Because we have shown that the BDHT pathway is much more favorable than *β*-H elimination for **3** dehydrogenation (*supra infra*), only BDHT mechanism was considered for the dehydrogenation of **18**. Similar to the **3** dehydrogenation (Figure 1), **TS10_OL** using alcohol **3** as an H-transfer shuttle is 10.3 kcal/mol lower than **TS10** for direct dehydrogenation (Figure 8). The dehydrogenation of **18** overcomes a 23.9 kcal/mol barrier and is endergonic by (+)7.2 kcal/mol. The values are compared with 21.9 and −4.3 kcal/mol (Figure 1) for the **3** dehydrogenation. Again the dehydrogenation of a primary alcohol is less favorable than the dehydrogenation of a secondary alcohol kinetically and thermodynamically. Nevertheless, the **18** dehydrogenation can occur, because the subsequent steps can drive the reaction forward due to the base promotion (*vide infra*).

After **18** dehydrogenation to give **24**, the base (**19**, $^tBuO^-$) acts, pulling off the methyl hydrogen (H^1). As shown in Figure 9, **19** first approaches **24** to form **25** via electrostatic attraction and then climbs **TS11** to give anionic **26**. The H^1 abstraction undergoes easily with a barrier of 2.6 kcal/mol and exergonicity of 6.2 kcal/mol relative to **24** + **19**. After rearranging to slightly more stable **27**, a C−C bond forms by a nucleophilic attack via **TS12**, giving the cyclic **28** with a five-membered ring formed. Relative to **27**, the ring closure crosses a 3.9 kcal/mol barrier and is exergonic by 12.6 kcal/mol. Subsequently, a dehydration process takes place via 1,3-H transfer to move H^2 to O^1, leading to **29**. The barrier (29.9 kcal/mol) for the direct 1,3-H transfer via **TS13** can also be reduced by an H-transfer shuttle. For example, if using one water molecule as a bridge (**TS13_W**), the barrier can be reduced to 13.7 kcal/mol. An alternative 1,3-H transfer moving H^3 to O^1 was found to be less favorable (**TS13′** and **TS13′_W** are higher than **TS13** and **TS13_W** by 3.8 and 4.5 kcal/mol, respectively). In **29**, a H_2O entity is formed. The dehydration completes via crossing a barrier of 9.1 kcal/mol (**TS14**), and the H_2O moiety leaves in the form of $^tBuO^-\cdots HOH$ (**23**), leading to **30** + **23**. Note that **30** is not the final product (pyrrole **5**) and requires a 1,2-H transfer to give pyrrole **5** (*vide infra*). In addition to grabbing H^1 to enable the C−C coupling, the base also benefits the step thermodynamically. The transformation of **24**→**30** + H_2O is exergonic by (−)9.2 kcal/mol, compared to the −17.0 kcal/mol for the transformation of **24** + **19**($^tBuO^-$) → **30** + **23**($^tBuO^-\cdots HOH$).

The energy profile for leading cyclic **30** to pyrrole **5** is shown in Figure 10, together with the optimized structures of key stationary points. The direct 1,2-H transfer passes a barrier (**TS15**) of 28.3 kcal/mol relative to **30**. Different from the various H-transfer processes discussed above, an H-transfer shuttle cannot facilitate this step. For example, a water H-transfer shuttle increases the barrier to 38.9 kcal/mol (**TS15_W** relative to **30** + H_2O). Interestingly, the 1,2-H transfer can occur much easier via intermolecular H-exchange. As shown by **TS16** and **TS17**, two **30** molecules interexchange H atoms sequentially. The overall barrier for the mechanism is 17.8 kcal/mol (**TS16**), which is significantly lower than the 28.3 kcal/mol for intramolecular 1,2-H transfer.

*3.1.4. Regeneration of the Active Catalyst (**1A**) from the Resting Catalyst (**1R**) (Stage IV).* The dehydrogenations of **3** (stage I) and **18** (stage III) transform the active catalyst **1A** to the PNP-Ir(III) trihydride (**1R**). To maintain catalysis, **1A** needs to be regenerated, which can be fulfilled by releasing H_2 from **1R**. Two H_2-elimination pathways were considered, as illustrated in Figures 11 and 13, respectively. Figure 11 describes the pathway to form molecular H_2 via eliminating the protonic H at N and hydridic H at Ir simultaneously. The direct H_2-elimination via **TS18** has a very high barrier (45.9 kcal/mol), and an H-transfer shuttle must act. The shuttle using one alcohol **3** can reduce the barrier to 33.9 kcal/mol (**TS18_1OL**) which can be further lowered to 24.2 kcal/mol (**TS18_2OL**) by using a shuttle of **3** dimer. **TS18** leads to a dihydrogen complex **32** which can release molecular H_2 via **TS19** with a barrier of 7.3 kcal/mol. As reflected by the $\angle IrN^1H^1$ angles in **TS18**(49.4°), **TS18_1OL**(81.9°) and **TS18_2OL**(122.2°) (see Figure 12), the H-transfer shuttles dramatically reduce the strain in the latter two TSs, which is responsible for the significantly decreased H_2-elimination barriers from 45.9 to 33.9 to 24.2 kcal/mol. Previously, Musgrave et al. have analyzed the role of H-transfer shuttle in reducing the strain in their case of proton transfer from PyH^0 + CO_2 to $PyCOOH^0$.[42]

For the second pathway (Figure 13), the two hydridic H atoms (H^3 and H^4) at Ir center are first eliminated, leading **1R** to **33**. The process crosses a barrier of 23.6 kcal/mol (**TS20**) and is endergonic by 7.0 kcal/mol after releasing H_2 to reach

dx.doi.org/10.1021/ja411568a | J. Am. Chem. Soc. 2014, 136, 4974−4991

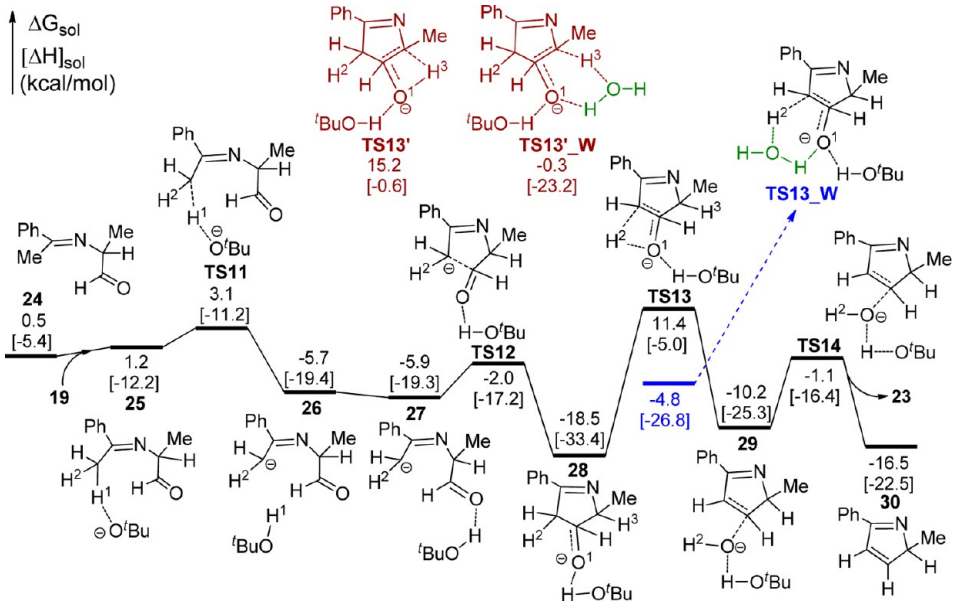

Figure 9. Pathway for base-promoted ring closure leading **24** to **30**, along with the relative free energies and enthalpies (in brackets). Optimized geometries of key stationary points see Figure S9.

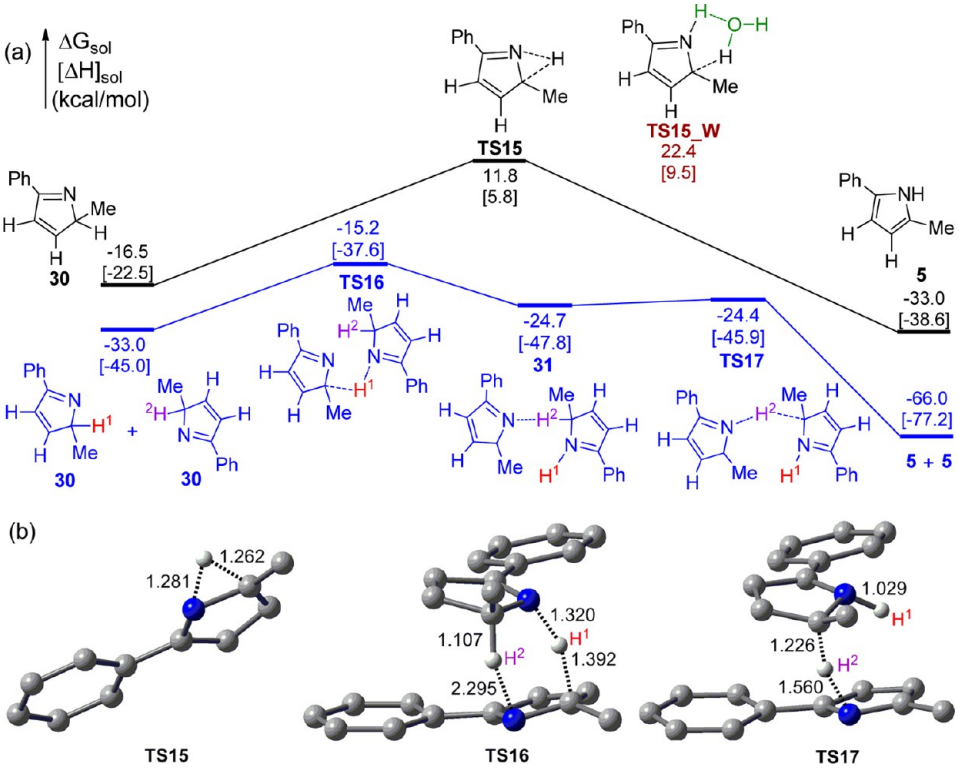

Figure 10. Pathways for leading **30** to **5** via direct intramolecular 1,2 H-transfer (black pathway in (a)) and intermolecular H-exchange (blue pathway in (a)), along with the relative free energies and enthalpies (in brackets); and optimized structures of key transition states (b). Key bond lengths are given in angstroms. Trivial H atoms are omitted for clarity.

14. However, the Ir(I) complex **14** cannot be an active catalyst to directly dehydrogenate alcohol, as mentioned above: As shown in Figure 14, the first H-transfer step involved in the complete dehydrogenation of **3**, mediated by **14**, is highly unfavorable kinetically (with a barrier of 40.2 kcal/mol relative to **3** + **14**) and thermodynamically (being endergonic by 13.7 kcal/mol). We did not further pursue the second H-transfer step. To regenerate **1A** from **14**, the H^1 at N needs to transfer to the Ir(I) center (see Figure 13). The barrier (**TS21**) for direct transfer is 53.2 kcal/mol relative to **14**, but this barrier can be reduced greatly to 25.0 kcal/mol (**TS21_2OL** relative to **14** + **3** + **3**), when **3** dimer participates as an H-transfer shuttle. The overall barrier for this pathway is 32.0 kcal/mol (**TS21_2OL** relative to **1R** + **3** + **3**), which is higher than the 24.2 kcal/mol of **TS18_2OL** on the pathway shown in Figure 11. The comparisons indicate the first pathway to be

dx.doi.org/10.1021/ja411568a | J. Am. Chem. Soc. 2014, 136, 4974−4991

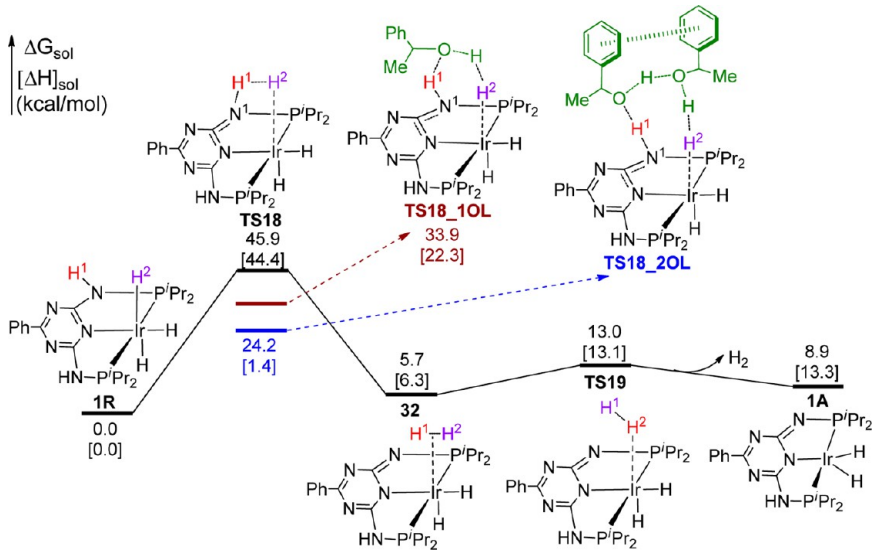

Figure 11. Pathway for catalyst regeneration via eliminating the protonic H on N and hydridic H on Ir, along with the relative free energies and enthalpies (in brackets).

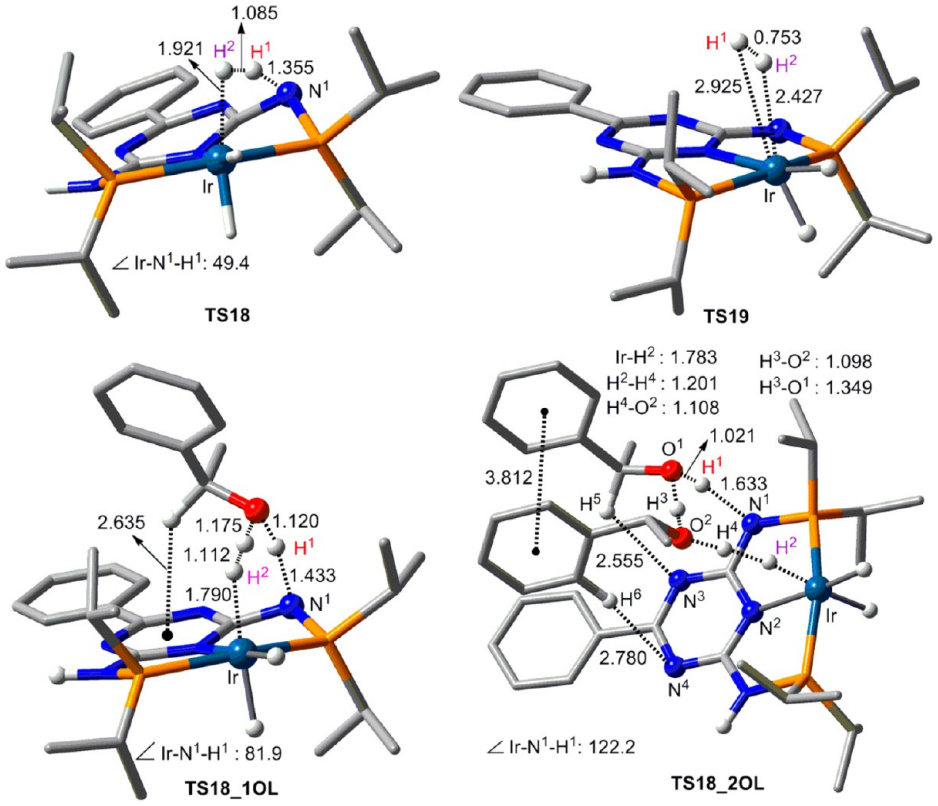

Figure 12. Optimized geometries of key stationary points labeled in Figure 11. Key bond lengths and angles are given in angstroms and degrees, respectively. Trivial H atoms are omitted for clarity.

preferred for leading **1R** to the active catalyst **1A** to complete the catalytic cycle. The moderate kinetic stability of **1R** explains why it could be crystallized as a resting state. In this stage we also used **4** to construct H-transfer shuttle. The results are given in Figure S12, which again show that **3** is more effective than **4**.

Assembling the four stages together, the highest barriers for each of the stages are 21.9, 10.3, 23.9, and 24.2 kcal/mol, respectively, indicating the kinetic feasibility of the catalytic cycle. The side reactions which may compete with the main pathway are less favorable and can be excluded safely. The whole transformation from **3** + **4** to **5** + $2H_2O$ + $2H_2$ is slightly endergonic by 0.3 kcal/mol. However, the involvement of a base in stages II and III can enhance the thermodynamics of the transformation; the transformation of **3** + **4** + 2 × ^{t}BuO$^-$ → **5** + $2H_2$ + 2 × **23**(^{t}BuO$^-$···HOH) is exergonic by 15.2 kcal/mol. One may ask that, if two base molecules are involved, but the experiments only used 1.1 (Kempe et al.'s study) or 0.5 (Milstein et al.'s study) equivalence of base (eq 1). This is

dx.doi.org/10.1021/ja411568a | J. Am. Chem. Soc. 2014, 136, 4974−4991

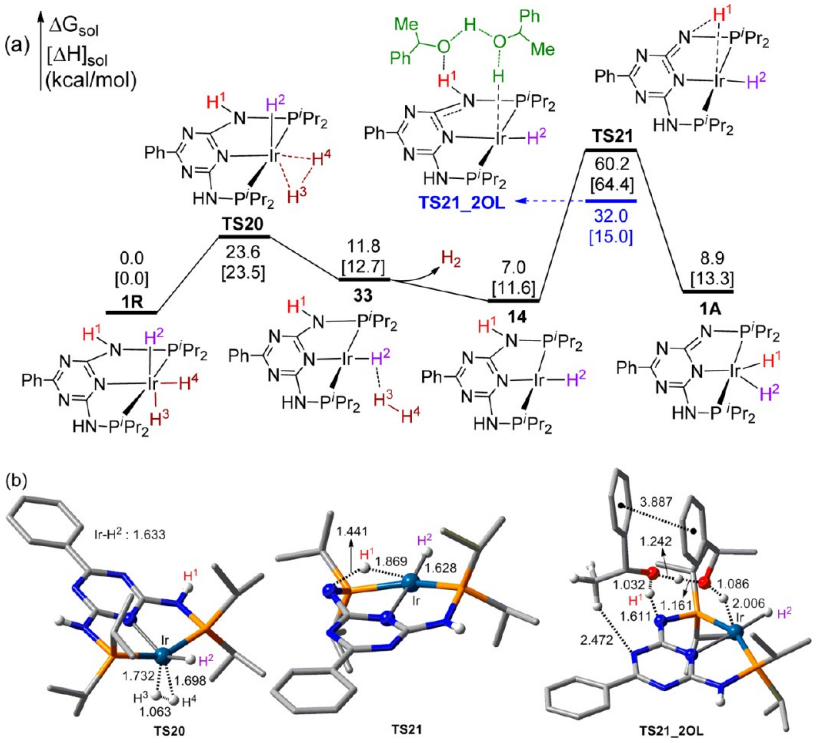

Figure 13. Pathway (a) for catalyst regeneration via first eliminating two hydridic H atoms on Ir(III) center, together with the relative free energies and enthalpies (in brackets); and optimized structures of key transition states (b). Bond lengths are given in angstroms, and trivial H atoms are omitted for clarity.

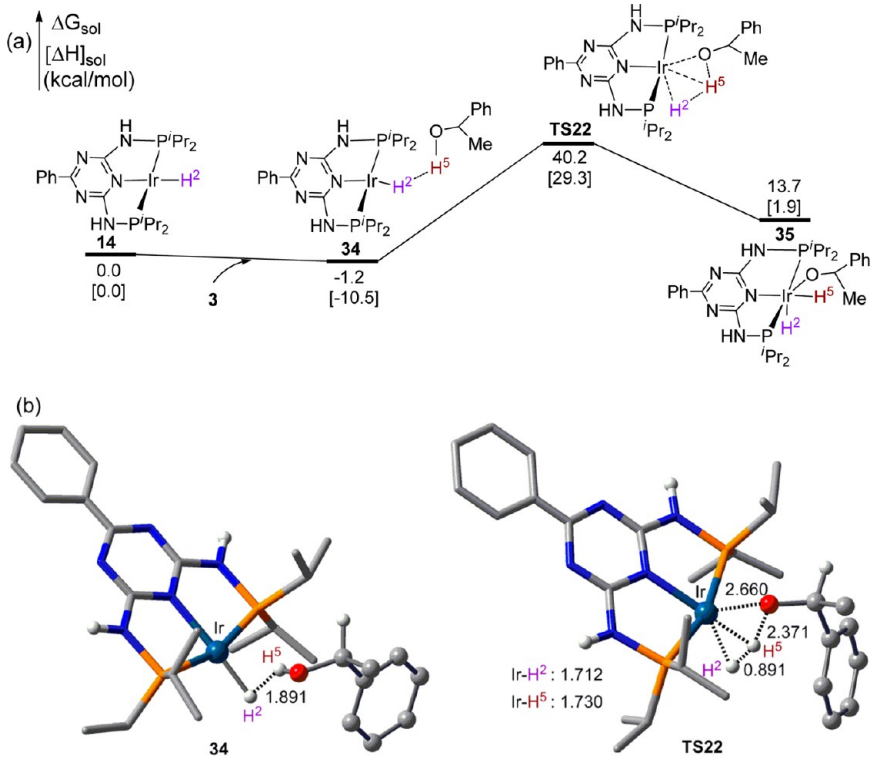

Figure 14. Energy profile alcohol dehydrogenation using **14** as active catalyst (a), together with the optimized structures of key stationary points (b). Key bond lengths are given in angstroms. Because of the high barrier of **TS22**, the step leading **35** to **11** + **1R** was not pursued.

because **23** can be dissociated to H_2O + $^tBuO^-$ at a energy cost of 7.8 kcal/mol, enabling to reuse the base.

3.2. Energetic Comparisons with That of PNN Pincer Ru Complex. Milstein et al. have shown that their PNN-Ru pincer complex (**2**) could also promote the production of pyrrole **5** from **3** and **4**. Referring to Scheme 2, after precatalyst (**2**) activation, the resulting active species **2A** catalyzes the transformation by following the same four stages. However,

dx.doi.org/10.1021/ja411568a | J. Am. Chem. Soc. 2014, 136, 4974−4991

because **1A** and **2A** have different metal−ligand active sites (═N···Ir in **1A** vs ═CH···Ru in **2A**), their energetics for the dehydrogenations of **3** and **18** and H_2-elimination are different. Table 1 compares the energetic results of the three steps, and Figure 15 shows the optimized structures of key transition states of these steps involved in **2A**-catalyzed transformation.

Table 1. Energetic Comparisons of the Dehydrogenations of 3 and 18 and H_2-Elimination Occurring in 1A- and 2A-Systems

	1A- system		2A-system	
	$[\Delta G]^{\ddagger a}$	ΔG^b	$[\Delta G]^{\ddagger a}$	ΔG^b
dehydrogenation of **3** (BDHT)	21.9(32.5)[c]	−4.3	4.2(13.4)	−4.1
dehydrogenation of **18** (BDHT)	23.9(34.2)	7.2	12.6(17.6)	7.4
H_2-elimination from **1R**/**2R**	24.2(45.9)	8.9	21.7(31.8)	8.7

[a]Free energy barriers (in kcal/mol) using monomeric alcohol **3** as an H-transfer shuttle except for H_2-elimination from **1R** which uses **3** dimer as shuttle. [b]Reaction energies in kcal/mol. [c]Values in the parentheses without using H-transfer shuttles.

The ΔG values in Table 1 indicate the thermodynamics of the three steps in the two systems are similar. However, H-transfer shuttles play a much more crucial role to enable the transformation in **1A**-system than in **2A**-system. In the case of **1A**-system, without using H-transfer shuttles, the barriers for the three steps are 32.5, 34.2, and 45.9 kcal/mol, respectively, which, in particular the barrier (45.9 kcal/mol) for H_2-elimination, are too high for experimental access. Only when H-transfer shuttles participate, the barriers can be reduced to the experimentally accessible heights (21.9, 23.9, and 24.2 kcal/mol, respectively). In the case of **2A**-system, H-transfer shuttles are able to reduce the barriers, but the barriers without using H-transfer shuttles are not too high (13.4, 17.6, and 31.8 kcal/mol). Again, for the dehydrogenation of **3** catalyzed by **2A**, the barrier via β-H elimination (18.2 kcal/mol, **TS25** relative to **3** + **2A**, see Figure S2) is higher than that via BDHT mechanism even without using an H-transfer shuttle (13.4 kcal/mol, see **TS23** in Figure S1). Notably, the β-H elimination barrier (18.2 kcal/mol) of **TS25** in **2A**-system is much lower than the corresponding value (39.7 kcal/mol) of **TS5** in **1A**-system (Figure 3). The large difference can be attributed to that both β-H elimination processes require the dissociation of one arm

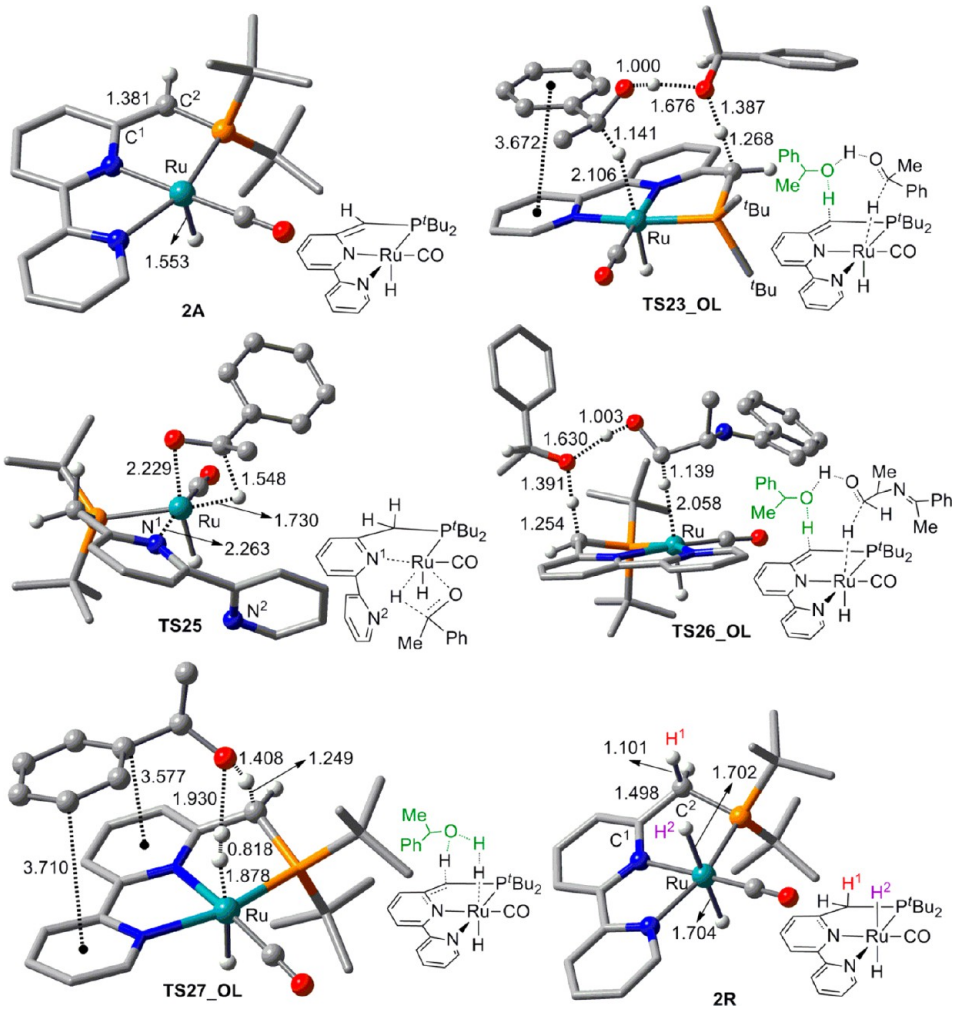

Figure 15. Optimized geometries of **2A** and **2R** and the key transition states involved in **2A**-catalyzed transformation. **TS23_OL** and **TS26_OL** are the TSs for the dehydrogenations of **3** and **18**, respectively. **TS25** is the key TS for the dehydrogenation of **3** via β-H elimination mechanism. **TS27_OL** is the TS for H_2-elimination. Key bond lengths are given in angstroms, and trivial H atoms are omitted for clarity.

dx.doi.org/10.1021/ja411568a | J. Am. Chem. Soc. 2014, 136, 4974−4991

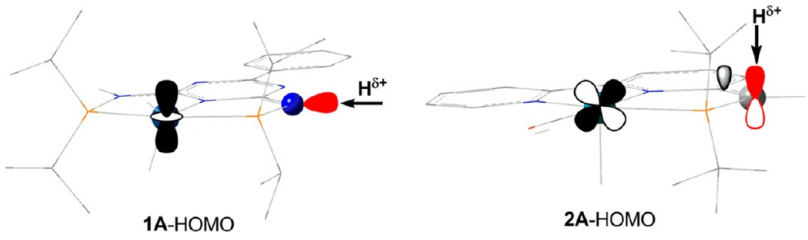

Figure 16. Schematic drawing of HOMOs of **1A** and **2A** with focus on the atomic orbitals of active sites. Complete drawings of FMOs of **1A** and **2A** are displayed in Figure S13.

Scheme 3. (a) Insertion vs BDHT Reaction Modes of CO_2 with 1R′/2R′/3R′ and (b) Alcohol Dehydrogenation via BDHT Pathway

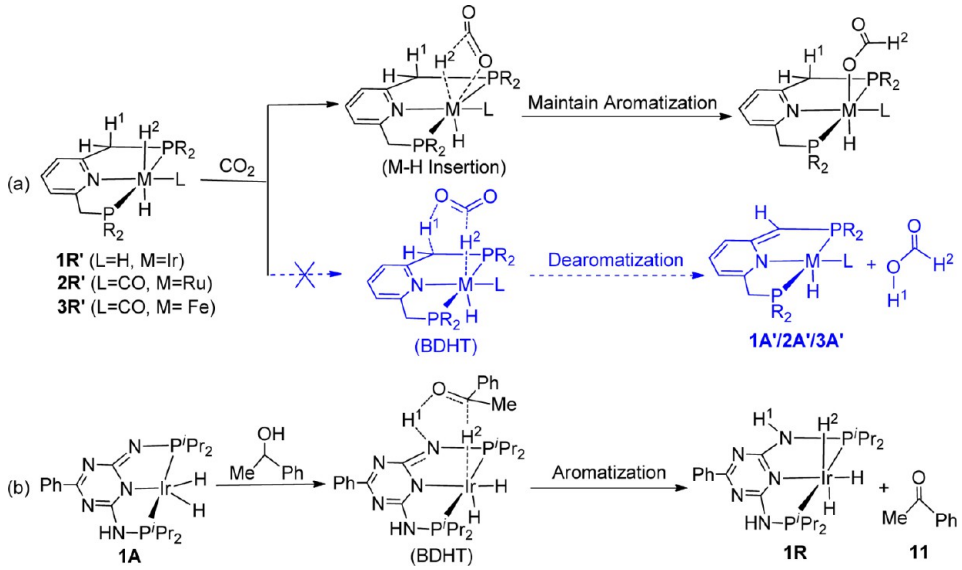

ligand, but the pyridine arm in **2A** is more labile than the −NH-P^{i}Pr$_2$ arm in **1A**.

The more crucial role of H-transfer shuttles in **1A**-system than in **2A**-system can be understood by comparing the HOMOs of **1A** and **2A**. As sketched in Figure 16, the lone-pair-like orbital on N in **1A**-HOMO lies in the C═N···Ir plane and is outward the Ir d_z^2 orbital, thus protonic $H^{\delta+}$ prefers attacking N from outward. To follow the preferred attacking direction, an H-shuttle is required for alcohol dehydrogenation. In contrast, the C═C π orbital is involved in **2A**-HOMO, allowing protonic $H^{\delta+}$ to attack C^2 from top; thus it is not necessary to have an H-transfer shuttle for alcohol dehydrogenation. Note that the C═N π orbital in **1A** is 0.26 eV below **1A**-HOMO (see Figure S13). For H_2-elimination, in **2R** the H^1 at sp^3 C is nearly parallel to the H^2 atom on Ru(II) center (Figure 15), while in **1R** the H^1 at the sp^3 N points away from the H^2 atom at Ir(III) (Figure 2). Consequently, an even longer H-transfer shuttle (**3** dimer) is necessary to lower the barrier (45.9 kcal/mol) to an accessible height (24.2 kca/mol). The barrier using **3** monomer shuttle is still somewhat high (33.9 kcal/mol, **TS18_1OL**). In comparison, **2R** only can fit a monomeric H-transfer shuttle (see **TS27_OL** in Figure 15). Previously, Huang et al. have demonstrated that Ru analogs of **2**, in which ═N− replaces ═CH− in the arms, could also catalyze similar dehydrogenation reactions.[45] We reason that similar H-transfer shuttles must act there.

The condition of **1A** requiring H-transfer shuttles to enable its activity is an interesting aspect, which may be utilized to develop catalysts that are less sensitive toward moisture. When such a catalyst is kept in a place where humidity is not high, H-transfer shuttles, in particular dimeric shuttles, cannot be formed easily, so the catalyst would be relatively stable. When the catalyst is applied to perform catalysis under conditions where H-transfer shuttles become readily available, the catalyst turns on its activity.

Compared to the direct H_2-elimnation via **TS27** (Table 1 and Figure S4), the H-transfer shuttle (**3**) in **TS27_OL** reduces the H_2-elimination barrier by 10.1 kcal/mol. Our previous study showed a methanol H-transfer shuttle did not reduce the H_2-elimination barrier from the hydride complex of **8** that much.[21d] We attribute the difference majorly to the $\pi-\pi$ interaction between the phenyl group of alcohol **3** and bipyridine ligand of **2A** (see **TS27_OL** in Figure 15), denoting as catalyst-shuttle $\pi-\pi$ interaction hereafter. To verify this, we calculated the H_2-elimination barriers, using water and 2-propanol as H-transfer shuttles, respectively. The barriers (32.8 and 27.5 kcal/mol, respectively, see **TS27_W** and **TS27_OL′** in Figure S4), compared to 21.7 kcal/mol of **TS27_OL**, verify the role of the catalyst-shuttle $\pi-\pi$ interaction. The features of **2A**, π-conjugation and the planarity of the pyridine arm (which also gives rise to less steric effect with a substrate than −NH-P^{i}Pr$_2$ in **1A**), are responsible for forming the catalyst-shuttle $\pi-\pi$ interaction. There is also similar catalyst-shuttle $\pi-\pi$ interaction in the dehydrogenation TS of **3** (**TS23_OL**) but no such $\pi-\pi$ interaction in the **18** dehydrogenation TS (**TS26_OL**), because there is no phenyl group at α-position

dx.doi.org/10.1021/ja411568a | J. Am. Chem. Soc. 2014, 136, 4974−4991

Table 2. Comparisons of Experimental Results of the Same Reactions Mediated by 1 and 2

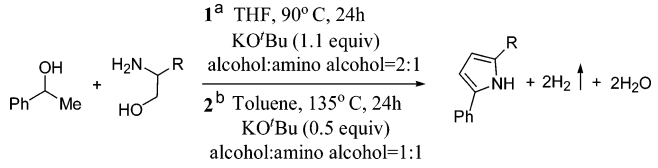

Entry	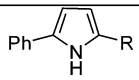	Ir-system		Ru-system	
		Catalyst loading (mol%)[a]	Yield (%)[a]	Catalyst loading (mol%)[b]	Yield (%)[b]
1	R=Me	0.05	80	0.5	71
2	R=Et	0.05	93	0.5	75
3	R=*i*-Pr	0.03	89	0.5	83
4	R=X[c]	0.05	88	0.5	67
5	R=Ph	0.2	86	0.5	62
6	R=*i*-Bu	0.1	69	0.5	78
7	R=Bn	0.05	79	0.5	85

[a]Run in a pressure tube closed with a semipermeable membrane. [b]Run in reflux apparatus. [c]X = 1-methylpropyl.[8,9]

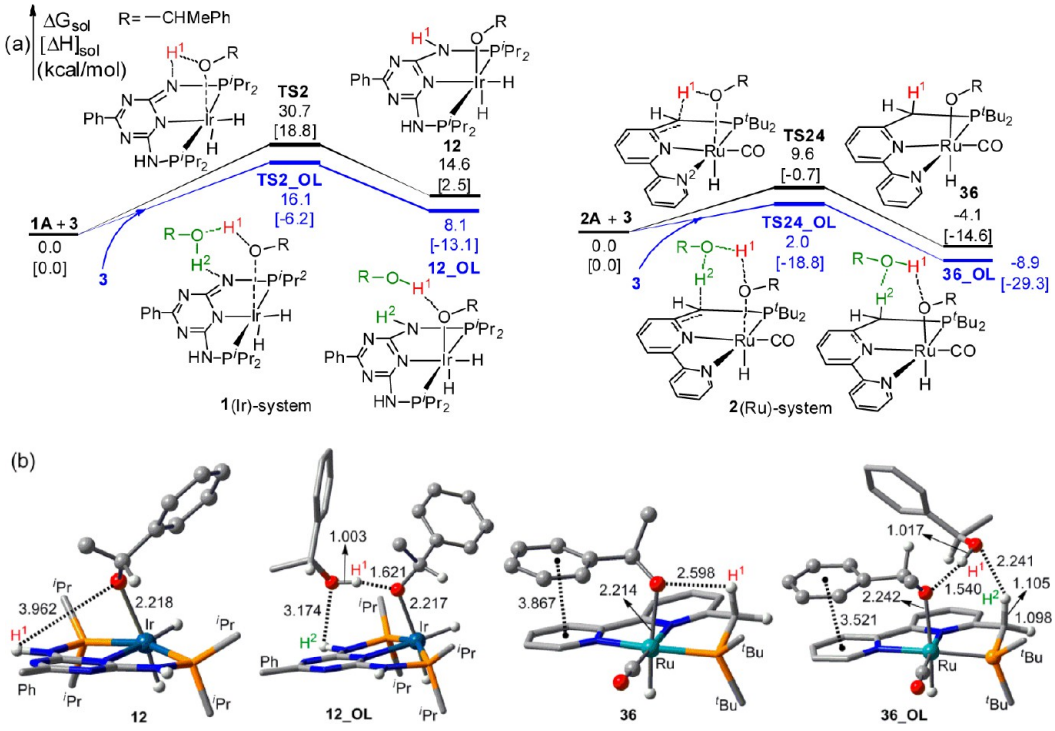

Figure 17. Energetic results of side reactions leading to alkoxo complexes (a), together with optimized structures of key stationary points (b). Bond lengths are given in angstroms, and trivial H atoms are omitted for clarity.

in **18** (a primary alcohol). Compared to **2A**, **1A** only contains one *s*-triazine ring, and both arm ligands (=N–P^{i}Pr$_2$ or –NH-P^{i}Pr$_2$) are sterically hindered, which is not suitable for forming catalyst-shuttle $\pi-\pi$ interaction, as shown by the structures of **TS1_OL**, **TS10_OL**, **TS18_1OL**, and **TS18_2OL.** However, there is an intrashuttle $\pi-\pi$ interaction between the two phenyl groups in the dimeric H-transfer shuttle in **TS18_2OL** (see Figure 12).

It has been shown that the Ir-, Ru-, and Fe-analogs of **1R** and **2R** (i.e., **1R′**/**2R′**/**3R′** in Scheme 3) are involved in the base-aided reduction of CO_2 with H_2.[25−28] Interestingly, as we predict the BDHT reaction model for alcohol dehydrogenation giving carbonyl compounds, studies have shown that CO_2 does

dx.doi.org/10.1021/ja411568a | J. Am. Chem. Soc. 2014, 136, 4974−4991

not react with these hydrides via BDHT hydrogenation process to result in formic acid and **1A′**/**2A′**/**3A′**.[27,29] Instead, CO_2 inserts into the metal-H bonds of **1R′**/**2R′**/**3R′** without disturbing the aromaticity of the pyridine ligand. The different reaction models can be understood as follow: If the reaction CO_2 with these hydrides via BDHT mechanism, both processes, resting state (**1R′**/**2R′**/**3R′**) → active state (**1A′**/**2A′**/**3A′**) (dearomatization) and $CO_2 + H_2$ → HCOOH, are energetically unfavorable, making the overall reaction unfavorable (Scheme 3a). In contrast, for the alcohol dehydrogenation via BDHT mechanism catalyzed by **1A**, the process (alcohol → ketone/or aldehyde + H_2) is energetically unfavorable, but the other process, active state (**1A**) → resting state (**1R**), is favorable due to aromatization (Scheme 3b). The latter process compensates the energetic loss of the former to make the reaction feasible.

Table 2 compares the experimental results of the same reactions mediated by **1** and **2**. It can be found that, compared to the **2**(Ru)-system, the **1**(Ir)-system tends to require lower catalyst loadings and can be performed at relatively lower temperature, but gives relatively higher yields except for entry 6 and 7. This trend is not in agreement with the computed energetic results in Table 1, which show that for the main reaction channel, the **1A**-catalyzed transformation is less kinetically favorable than the **2A**-catalyzd one. Because these reactions were run by different groups under different experimental conditions, many factors could contribute to the different yields. However, from an energetic point of view, we can identify a key factor (a side reaction) that could be responsible for the energetic inconsistency. These transformations all used alcohols as reactants. In addition to promoting alcohol dehydrogenations through BDHT mechanism, as a side reaction, the active catalysts (**1A** or **2A**) also probably break alcohol O−H bond via addition to the active sites (i.e., =N···Ir in **1A** and =CH···Ru in **2A**), resulting in alkoxo complexes. As an example, Figure 17 compares the energetics for these side reactions of **1A** and **2A** with alcohol **3**. Regardless of whether to use H-transfer shuttle or not, the side reactions in both systems are kinetically feasible with that in Ru-system being more favorable, but are quite different thermodynamically. If H-transfer shuttle is involved, the side reaction in the **1**-system is uphill by 8.1 kcal/mol, whereas that in the **2**-system is downhill by 8.9 kcal/mol. The readily formations of the relative stable alkoxo complexes (**36** or **36_OL**) in **2**-system would lower the concentration of the active species **2A**, thus requiring relatively large catalyst loading for effective transformations in this system. Note that Milstein et al. have experimentally detected similar alkoxo complexes in a similar Ru-system.[24] In contrast, the alkoxo complexes (**12** and **12_OL**) cannot be formed in **1**-system due to the unfavorable thermodynamics of the side reaction, so the side reaction would not influence the main reaction channel in **1**-system. In addition to these side reactions, the contribution of the difference in the ratio of substrates should be mentioned. In **1**-system, a ratio of 2:1 of the secondary alcohol to amino alcohol was applied, compared to a ratio of 1:1 in **2**-system. The excess secondary alcohol in **1**-system benefits the transformations in terms of reaction equilibrium and the availability of H-transfer shuttle as well. However, we reasoned that using excess alcohol in the **2**-system may not work as well as in **1**-system, because the excess alcohol can also promote formation of alkoxo complexes via the side reaction discussed above and H-shuttles are less crucial than those in **1**-system.

The less favorable thermodynamics of the side reaction of **1A** + **3** than that of **2A** + **3** can be understood by comparing the structures of **12**/**12_OL** with **36**/**36_OL**; as shown by their optimized structures (Figure 17b), the protonic H^1 in **12** points away from the $O^{\delta-}$ with $H^1-O^{\delta-}$ distance of 3.962 Å, while the positively charged H^1 in **36** is toward the $O^{\delta-}$ ($R(H^1-O^{\delta-})$ = 2.598 Å). If including an H-transfer shuttle (**3**), the shuttle in **36_OL** forms two H-bonds but only one in **12_OL**. Another factor is the steric effect: the alkoxy group of **12**/**12_OL** locates between the two bulky $-P^iPr_2$ ligands, while **36**/**36_OL** has open site in the side of pyridine arm. For the present case, the $\pi-\pi$ interaction in **36**/**36_OL** also contributes to the favorable thermodynamics of the side reactions, but it is not a determining factor to results in the different thermodynamics. For example, the side reaction of **1A** with the primary alcohol **4** is also thermodynamically less favorable than that of **2A** with **4** (see Figure S10 for details).

4. CONCLUSIONS

In summary, we have performed a density functional theory study to gain insight into the catalytic mechanism of the pyrrole synthesis from secondary alcohol (i.e., **3**) and β-amino alcohol (**4**) via dehydrogenative coupling, catalyzed by PNP-Ir and PNN-Ru pincer complexes. For the PNP-Ir system, the active catalyst is identified to be a PNP-Ir(III) dihydride (**1A**) rather than a PNP-Ir(I) complex (**14** in Figure 14). Under the catalysis of **1A**, the cycle for catalytically producing pyrrole proceeds via four stages, including alcohol (**3**) dehydrogenation, resulting in reactive ketone **11**; C−N coupling via condensation, forming imine-alcohol intermediate (**18**); intramolecular cyclization of **18** via dehydrogenation of **18**, base-promoted C−C coupling giving **30**, and 1,2-H transfer to deliver pyrrole (**5**); and catalyst regeneration via H_2-elimination from **1R**. In addition to showing the transformation to be energetically feasible and the side reactions are not competitive, the study reveals mechanistic details which may not be observed experimentally, which, among others, include: (a) Alcohol dehydrogenation prefers BDHT pathway over β-H elimination pathway, which is similar to the case catalyzed by analogs of PNN-Ru complex (**8**).[20v,21d] (b) The addition of alcohol O−H bond to **1A** giving an alkoxo complex is uphill by 8.1 kcal/mol, whereas the addition to **2A** is downhill by 8.9 kcal/mol. The significant thermodynamic difference of the side reactions could be the main reason for requiring smaller catalyst loading in Ir-system than in Ru-system. (c) Because the N lone pair of the $=N-P^iPr_2$ arm in **1A** is coplanar with the five-membered arm ring and points outward the vacant site of Lewis acidic Ir(III) center, H-transfer shuttles play an important role in reducing the dehydrogenation barriers of **3** and **18**. The barriers without H-transfer shuttles (32.5 and 34.2 kcal/mol, respectively) can be greatly reduced to 21.9 and 23.9 kcal/mol, respectively, when H-transfer shuttles are involved. For H_2-elimination, because the H^N on $-NH-P^iPr_2$ arm of **1R** points away from the H^{Ir} at Ir(III) and H_2 is small, an even longer dimeric H-transfer shuttle is necessary to reduce the barrier to an experimentally accessible value (24.2 kcal/mol). However, the indispensable necessity for H-transfer shuttles cannot shut off the transformation, because H-transfer shuttles are readily available from the system. The character of **1A** using an H-transfer shuttle to enable catalyst activity may suggest a strategy to develop catalysts that are less sensitive toward moisture. (d) The base not only plays a role in enabling ring closure by grabbing a methyl hydrogen but also promotes the coupling of

dx.doi.org/10.1021/ja411568a | J. Am. Chem. Soc. 2014, 136, 4974−4991

4 with 11 and benefits the thermodynamics of the whole transformation via forming $^{t}BuO^{-}\cdots H_2O$ complex. (e) For pyrrole formation from cyclic 30, the direct intramolecular 1,2-H transfer is kinetically difficult with a barrier of 28.2 kcal/mol, while the intermolecular H-exchange is much more facile with a barrier of 17.8 kcal/mol. The transformation catalyzed by 2A follows the similar four stages except for the energetic differences in the dehydrogenations and H_2-elimination. Because the proper geometric arrangement of the $=$CH-P^{t}Bu$_2$ arm in 2A and $-CH_2$-P^{t}Bu$_2$ arm in 2R, H-transfer shuttles play less important role in the alcohol dehydrogenations and H_2-eliminaiton, although H-transfer shuttles can also lower the barriers.

■ ASSOCIATED CONTENT

Supporting Information

Additional computational results, total energies, and Cartesian coordinates of all optimized structures. This information is available free of charge via the Internet at http://pubs.acs.org.

■ AUTHOR INFORMATION

Corresponding Author

zxwang@ucas.ac.cn

Notes

The authors declare no competing financial interest.

■ ACKNOWLEDGMENTS

This work is financially supported by National Natural Science Foundation of China (nos. 21173263 and 21373216). We greatly appreciate the insightful suggestions of the anonymous reviewers which helped us to improve the study.

■ REFERENCES

(1) (a) Gunanathan, C.; Milstein, D. *Science* **2013**, *341*, 249. (b) Marr, A. C. *Catal. Sci. Technol.* **2012**, *2*, 279. (c) Gunanathan, C.; Milstein, D. *Acc. Chem. Res.* **2011**, *44*, 588. (d) Choi, J.; MacArthur, A. H.; Brookhart, M.; Goldman, A. S. *Chem. Rev.* **2011**, *111*, 1761. (e) Bower, J. F.; Krische, M. J. *Top. Organomet. Chem.* **2011**, *34*, 107. (f) Watson, A. J.; Williams, J. M. *Science* **2010**, *329*, 635. (g) Dobereiner, G. E.; Crabtree, R. H. *Chem. Rev.* **2009**, *110*, 681.

(2) (a) Gunanathan, C.; Ben-David, Y.; Milstein, D. *Science* **2007**, *317*, 790. (b) Nordstrøm, L. U.; Vogt, H.; Madsen, R. *J. Am. Chem. Soc.* **2008**, *130*, 17672. (c) Chen, C.; Zhang, Y.; Hong, S. H. *J. Org. Chem.* **2011**, *76*, 10005. (d) Zeng, H.; Guan, Z. *J. Am. Chem. Soc.* **2011**, *133*, 1159.

(3) (a) Gnanaprakasam, B.; Zhang, J.; Milstein, D. *Angew. Chem., Int. Ed.* **2010**, *49*, 1468. (b) Gnanaprakasam, B.; Balaraman, E.; Ben-David, Y.; Milstein, D. *Angew. Chem.* **2011**, *123*, 12448; *Angew. Chem., Int. Ed.* **2011**, *50*, 12240.

(4) (a) Zhang, J.; Leitus, G.; Ben-David, Y.; Milstein, D. *J. Am. Chem. Soc.* **2005**, *127*, 10840. (b) Spasyuk, D.; Smith, S.; Gusev, D. G. *Angew. Chem., Int. Ed.* **2012**, *51*, 2772. (c) Spasyuk, D.; Gusev, D. G. *Organometallics* **2012**, *31*, 5239. (d) Nielsen, M.; Junge, H.; Kammer, A.; Beller, M. *Angew. Chem., Int. Ed.* **2012**, *51*, 5711. (e) Gunanathan, C.; Shimon, L. J. W.; Milstein, D. *J. Am. Chem. Soc.* **2009**, *131*, 3146. (f) Kossoy, E.; Diskin-Posner, Y.; Leitus, G.; Milstein, D. *Adv. Synth. Catal.* **2012**, *354*, 497.

(5) Schley, N. D.; Dobereiner, G. E.; Crabtree, R. H. *Organometallics* **2011**, *30*, 4174.

(6) Zhang, M.; Neumann, H.; Beller, M. *Angew. Chem., Int. Ed.* **2013**, *52*, 597.

(7) Zhang, M.; Fang, X.; Neumann, H.; Beller, M. *J. Am. Chem. Soc.* **2013**, *135*, 11384.

(8) Michlik, S.; Kempe, R. *Nat. Chem.* **2013**, *5*, 140.

(9) Srimani, D.; Ben-David, Y.; Milstein, D. *Angew. Chem., Int. Ed.* **2013**, *52*, 4012.

(10) (a) Amishiro, N.; Nagamura, S.; Kobayashi, E.; Okamoto, A.; Gomi, K.; Saito, H. *Chem. Pharm. Bull.* **1999**, *47*, 1393. (b) Amishiro, N.; Nagamura, S.; Kobayashi, E.; Okamoto, A.; Gomi, K.; Okabe, M.; Saito, H. *Bioorg. Med. Chem.* **2000**, *8*, 1637. (c) Demopoulos, V. J.; Rekka, E. *J. Pharm. Sci.* **1995**, *84*, 79. (d) Bürli, R. W.; McMinn, D.; Kaizerman, J. A.; Hu, W.; Ge, Y.; Pack, Q.; Jiang, V.; Gross, M.; Garcia, M.; Tanaka, R.; Moser, H. E. *Bioorg. Med. Chem. Lett.* **2004**, *14*, 1253. (e) Wang, D.; Hu, X.; Zhao, G. *Int. J. Food Sci. Technol.* **2008**, *43*, 1880. (f) Wang, M.-Z.; Xu, H.; Liu, T.-W.; Feng, Q.; Yu, S.-J.; Wang, S.-H.; Li, Z.-M. *Eur. J. Med. Chem.* **2011**, *46*, 1463. (g) Del Poeta, M.; Schell, W. A.; Dykstra, C. C.; Jones, S.; Tidwell, R. R.; Czarny, A.; Bajic, M.; Kumar, A.; Boykin, D.; Perfect, J. R. *Antimicrob. Agents Chemother.* **1998**, *42*, 2495.

(11) Joule, J. A.; Mills, K. *Heterocyclic Chemistry*, 5th ed.; Wiley: New York, 2010.

(12) (a) Pfluger, P.; Krounbi, M.; Street, G. B.; Weiser, G. *J. Chem. Phys.* **1983**, *78*, 3212. (b) Gimenez, I. F.; Alves, O. L. *J. Braz. Chem. Soc.* **1999**, *10*, 167. (c) Reynolds, J. R.; Poropatic, P. A.; Toyooka, R. L. *Macromolecules* **1987**, *20*, 958.

(13) (a) Niziurskimann, R. E.; Cava, M. P. *Heterocycles* **1992**, *34*, 2003. (b) Chou, S.-S. P.; Yeh, Y.-H. *Tetrahedron Lett.* **2001**, *42*, 1309.

(14) D'Silva, C.; Walker, D. A. *J. Org. Chem.* **1998**, *63*, 6715.

(15) (a) Trautwein, A. W.; Süßmuth, R. D.; Jung, G. *Bioorg. Med. Chem. Lett.* **1998**, *8*, 2381. (b) Calvo, L.; Gonzalez-Ortega, A.; Sanudo, M. C. *Synthesis* **2002**, 2450. (c) Matiychuk, V. S.; Martyak, R. L.; Obushak, N. D.; Ostapiuk, Y. V.; Pidlypnyi, N. I. *Chem. Heterocycl. Compd.* **2004**, *40*, 1218.

(16) (a) Alberola, A.; González Ortega, A.; Luisa Sádaba, M.; Sañudo, C. *Tetrahedron* **1999**, *55*, 6555. (b) Elghamry, I. *Synth. Commun.* **2002**, *32*, 897. (c) Manley, J. M.; Kalman, M. J.; Conway, B. G.; Ball, C. C.; Havens, J. L.; Vaidyanathan, R. *J. Org. Chem.* **2003**, *68*, 6447. (d) Bellingham, R. K.; Carey, J. S.; Hussain, N.; Morgan, D. O.; Oxley, P.; Powling, L. C. *Org. Process Res. Dev.* **2004**, *8*, 279. (e) Shiner, C. M.; Lash, T. D. *Tetrahedron* **2005**, *61*, 11628.

(17) (a) Chiu, P.-K.; Lui, K.-H.; Maini, P. N.; Sammes, M. P. *J. Chem. Soc., Chem. Commun.* **1987**, 109. (b) Chiu, P. K.; Sammes, M. P. *Tetrahedron* **1990**, *46*, 3439. (c) Banik, B. K.; Samajdar, S.; Banik, I. *J. Org. Chem.* **2003**, *69*, 213. (d) Chen, J.; Wu, H.; Zheng, Z.; Jin, C.; Zhang, X.; Su, W. *Tetrahedron Lett.* **2006**, *47*, 5383. (e) Minetto, G.; Raveglia, L. F.; Sega, A.; Taddei, M. *Eur. J. Org. Chem.* **2005**, *2005*, 5277.

(18) (a) Shiraishi, H.; Nishitani, T.; Sakaguchi, S.; Ishii, Y. *J. Org. Chem.* **1998**, *63*, 6234. (b) Nishibayashi, Y.; Yoshikawa, M.; Inada, Y.; Milton, M. D.; Hidai, M.; Uemura, S. *Angew. Chem., Int. Ed.* **2003**, *42*, 2681. (c) Dhawan, R.; Arndtsen, B. A. *J. Am. Chem. Soc.* **2003**, *126*, 468. (d) Tejedor, D.; González-Cruz, D.; García-Tellado, F.; Marrero-Tellado, J. J.; Rodríguez, M. L. *J. Am. Chem. Soc.* **2004**, *126*, 8390. (e) Yamamoto, Y.; Hayashi, H.; Saigoku, T.; Nishiyama, H. *J. Am. Chem. Soc.* **2005**, *127*, 10804. (f) Larionov, O. V.; de Meijere, A. *Angew. Chem., Int. Ed.* **2005**, *44*, 5664. (g) St. Cyr, D. J.; Martin, N.; Arndtsen, B. A. *Org. Lett.* **2007**, *9*, 449. (h) Shimizu, M.; Takahashi, A.; Kawai, S. *Org. Lett.* **2006**, *8*, 3585. (i) Bergner, I.; Opatz, T. *J. Org. Chem.* **2007**, *72*, 7083. (j) Galliford, C. V.; Scheidt, K. A. *J. Org. Chem.* **2007**, *72*, 1811. (k) Khalili, B.; Jajarmi, P.; Eftekhari-Sis, B.; Hashemi, M. M. *J. Org. Chem.* **2008**, *73*, 2090. (l) Merkul, E.; Boersch, C.; Frank, W.; Mueller, T. J. J. *Org. Lett.* **2009**, *11*, 2269. (m) Chen, X.; Hou, L.; Li, X. *Synlett* **2009**, 828. (n) Lu, Y.; Fu, X.; Chen, H.; Du, X.; Jia, X.; Liu, Y. *Adv. Synth. Catal.* **2009**, *351*, 129.

(19) (a) Kel'in, A. V.; Sromek, A. W.; Gevorgyan, V. *J. Am. Chem. Soc.* **2001**, *123*, 2074. (b) Braun, R. U.; Zeitler, K.; Muller, T. J. J. *Org. Lett.* **2001**, *3*, 3297. (c) Takaya, H.; Kojima, S.; Murahashi, S.-I. *Org. Lett.* **2001**, *3*, 421. (d) Wang, Y.; Zhu, S. *Org. Lett.* **2003**, *5*, 745. (e) Ramanathan, B.; Keith, A. J.; Armstrong, D.; Odom, A. L. *Org. Lett.* **2004**, *6*, 2957. (f) Siriwardana, A. I.; Kathriarachchi, K. K. A. D. S.; Nakamura, I.; Gridnev, I. D.; Yamamoto, Y. *J. Am. Chem. Soc.* **2004**, *126*, 13898. (g) Kamijo, S.; Kanazawa, C.; Yamamoto, Y. *J. Am. Chem. Soc.* **2005**, *127*, 9260. (h) Gorin, D. J.; Davis, N. R.; Toste, F. D. *J. Am.*

Chem. Soc. **2005**, *127*, 11260. (i) Wurz, R. P.; Charette, A. B. *Org. Lett.* **2005**, *7*, 2313. (j) Martín, R.; Rodríguez Rivero, M.; Buchwald, S. L. *Angew. Chem., Int. Ed.* **2006**, *45*, 7079. (k) Lu, L.; Chen, G.; Ma, S. *Org. Lett.* **2006**, *8*, 835. (l) Binder, J. T.; Kirsch, S. F. *Org. Lett.* **2006**, *8*, 2151. (m) Hiroya, K.; Matsumoto, S.; Ashikawa, M.; Ogiwara, K.; Sakamoto, T. *Org. Lett.* **2006**, *8*, 5349. (n) Istrate, F. M.; Gagosz, F. *Org. Lett.* **2007**, *9*, 3181. (o) Shu, X.-Z.; Liu, X.-Y.; Xiao, H.-Q.; Ji, K.-G.; Guo, L.-N.; Liang, Y.-M. *Adv. Synth. Catal.* **2008**, *350*, 243. (p) Aponick, A.; Li, C.-Y.; Malinge, J.; Marques, E. F. *Org. Lett.* **2009**, *11*, 4624. (q) Maiti, S.; Biswas, S.; Jana, U. *J. Org. Chem.* **2010**, *75*, 1674. (r) Liu, W.; Jiang, H.; Huang, L. *Org. Lett.* **2009**, *12*, 312. (s) Gao, M.; He, C.; Chen, H.; Bai, R.; Cheng, B.; Lei, A. *Angew. Chem., Int. Ed.* **2013**, *52*, 6958. (t) Ke, J.; He, C.; Liu, H.; Li, M.; Lei, A. *Chem. Commun.* **2013**, *49*, 7549. (u) Meng, L.; Wu, K.; Liu, C.; Lei, A. *Chem. Commun.* **2013**, *49*, 5853.

(20) (a) Iron, M. A.; Ben-Ari, E.; Cohen, R.; Milstein, D. *Dalton Trans* **2009**, 9433. (b) Schwartsburd, L.; Iron, M. A.; Konstantinovski, L.; Diskin-Posner, Y.; Leitus, G.; Shimon, L. J. W.; Milstein, D. *Organometallics* **2010**, *29*, 3817. (c) Paul, A.; Musgrave, C. B. *Angew. Chem., Int. Ed.* **2007**, *46*, 8153. (d) Zimmerman, P. M.; Paul, A.; Zhang, Z.; Musgrave, C. B. *Angew. Chem., Int. Ed.* **2009**, *48*, 2201. (e) Niu, S.; Hall, M. B. *J. Am. Chem. Soc.* **1999**, *121*, 3992. (f) Cui, X.; Fan, Y.; Hall, M. B.; Burgess, K. *Chem.—Eur. J.* **2005**, *11*, 6859. (g) Yang, X.; Hall, M. B. *J. Am. Chem. Soc.* **2009**, *132*, 120. (h) Balcells, D.; Nova, A.; Clot, E.; Gnanamgari, D.; Crabtree, R. H.; Eisenstein, O. *Organometallics* **2008**, *27*, 2529. (i) Krogh-Jespersen, K.; Czerw, M.; Summa, N.; Renkema, K. B.; Achord, P. D.; Goldman, A. S. *J. Am. Chem. Soc.* **2002**, *124*, 11404. (j) Zhu, K.; Achord, P. D.; Zhang, X.; Krogh-Jespersen, K.; Goldman, A. S. *J. Am. Chem. Soc.* **2004**, *126*, 13044. (k) Cantillo, D. *Eur. J. Inorg. Chem.* **2011**, *2011*, 3008. (l) Sandhya, K. S.; Suresh, C. H. *Organometallics* **2013**, *32*, 2926. (m) Hasanayn, F.; Baroudi, A. *Organometallics* **2013**, *32*, 2493. (n) Zeng, G.; Li, S. *Inorg Chem* **2011**, *50*, 10572. (o) Johansson, A. J.; Zuidema, E.; Bolm, C. *Chem.—Eur. J.* **2010**, *16*, 13487. (p) Muniz Filho, R. C. D.; de Moura, E. M.; de Souza, A. A.; Rocha, W. R. *Theochem-J. Mol. Struct.* **2007**, *816*, 77. (q) Sieffert, N.; Bühl, M. *J. Am. Chem. Soc.* **2010**, *132*, 8056. (r) Johansson, A. J.; Zuidema, E.; Bolm, C. *Chem.—Eur. J.* **2010**, *16*, 13487. (s) Fristrup, P.; Tursky, M.; Madsen, R. *Org. Biomol. Chem.* **2012**, *10*, 2569. (t) Li, J.; Shiota, Y.; Yoshizawa, K. *J. Am. Chem. Soc.* **2009**, *131*, 13584. (u) Chen, Y.; Fang, W.-H. *J. Phys. Chem. A* **2010**, *114*, 10334. (v) Cho, D.; Ko, K. C.; Lee, J. Y. *Organometallics* **2013**, *32*, 4571. (w) Li, H.; Hall, M. B. *J. Am. Chem. Soc.* **2013**, *136*, 383. (x) Yang, X. *ACS Catal.* **2013**, *3*, 2684. (y) Yang, X. *ACS Catal.* **2014**, *4*, 1129. (z) Zeng, G.; Sakaki, S.; Fujita, K.-i.; Sano, H.; Yamaguchi, R. *ACS Catal.* **2014**, *4*, 1010.

(21) (a) Li, H.; Lu, G.; Jiang, J.; Huang, F.; Wang, Z.-X. *Organometallics* **2011**, *30*, 2349. (b) Li, H.; Jiang, J.; Lu, G.; Huang, F.; Wang, Z.-X. *Organometallics* **2011**, *30*, 3131. (c) Li, H.; Wen, M.; Wang, Z. X. *Inorg Chem* **2012**, *51*, 5716. (d) Li, H.; Wang, X.; Huang, F.; Lu, G.; Jiang, J.; Wang, Z.-X. *Organometallics* **2011**, *30*, 5233. (e) Li, H.; Wang, X.; Wen, M.; Wang, Z.-X. *Eur. J. Inorg. Chem.* **2012**, *2012*, 5011. (f) Li, H.; Wang, Z. *Sci. China-Chem.* **2012**, *55*, 1991.

(22) (a) Yamaguchi, R.; Ikeda, C.; Takahashi, Y.; Fujita, K.-i. *J. Am. Chem. Soc.* **2009**, *131*, 8410. (b) Fujita, K.-i.; Tanino, N.; Yamaguchi, R. *Org. Lett.* **2007**, *9*, 109.

(23) (a) Wang, Z. X.; Zhao, L.; Lu, G.; Li, H.; Huang, F. *Top Curr Chem* **2013**, *332*, 231. (b) Lu, G.; Li, H.; Zhao, L.; Huang, F.; Schleyer, P. v. R.; Wang, Z.-X. *Chem.—Eur. J.* **2011**, *17*, 2038. (c) Li, H.; Wen, M.; Lu, G.; Wang, Z. X. *Dalton Trans* **2012**, *41*, 9091.

(24) Montag, M.; Zhang, J.; Milstein, D. *J. Am. Chem. Soc.* **2012**, *134*, 10325.

(25) (a) Tanaka, R.; Yamashita, M.; Nozaki, K. *J. Am. Chem. Soc.* **2009**, *131*, 14168. (b) Federsel, C.; Jackstell, R.; Beller, M. *Angew. Chem., Int. Ed.* **2010**, *49*, 6254.

(26) Fujita, E.; Muckerman, J. T.; Himeda, Y. *Biochim. Biophys. Acta, Bioenerg.* **2013**, *1827*, 1031.

(27) Langer, R.; Diskin-Posner, Y.; Leitus, G.; Shimon, L. J.; Ben-David, Y.; Milstein, D. *Angew. Chem., Int. Ed.* **2011**, *50*, 9948.

(28) Filonenko, G. A.; Conley, M. P.; Copéret, C.; Lutz, M.; Hensen, E. J. M.; Pidko, E. A. *ACS Catal.* **2013**, 2522.

(29) (a) Yang, X. *ACS Catal.* **2011**, *1*, 849. (b) Tanaka, R.; Yamashita, M.; Chung, L. W.; Morokuma, K.; Nozaki, K. *Organometallics* **2011**, *30*, 6742. (c) Ahlquist, M. S. G. *J. Mol. Catal. A: Chem.* **2010**, *324*, 3.

(30) (a) Kulkarni, A. D.; Truhlar, D. G. *J. Chem. Theory Comput.* **2011**, *7*, 2325. (b) Sliwa, P.; Handzlik, J. *Chem. Phys. Lett.* **2010**, *493*, 273. (c) Zhao, Y.; Truhlar, D. G. *J. Chem. Theory Comput.* **2009**, *5*, 324. (d) Zhao, Y.; Truhlar, D. G. *Acc. Chem. Res.* **2008**, *41*, 157.

(31) (a) Gordon, M. S. *Chem. Phys. Lett.* **1980**, *76*, 163. (b) Harihara, Pc; Pople, J. A. *Mol. Phys.* **1974**, *27*, 209. (c) Harihara, Pc; Pople, J. A. *Theor. Chem. Acc.* **1973**, *28*, 213. (d) Hehre, W. J.; Ditchfield, R.; Pople, J. A. *J. Chem. Phys.* **1972**, *56*, 2257. (e) Ditchfield, R.; Hehre, W. J.; Pople, J. A. *J. Chem. Phys.* **1971**, *54*, 724.

(32) (a) Roy, L. E.; Hay, P. J.; Martin, R. L. *J. Chem. Theory Comput.* **2008**, *4*, 1029. (b) Andrae, D.; Haussermann, U.; Dolg, M.; Stoll, H.; Preuss, H. *Theor. Chem. Acc.* **1990**, *77*, 123.

(33) Marenich, A. V.; Cramer, C. J.; Truhlar, D. G. *J. Phys. Chem. B* **2009**, *113*, 6378.

(34) (a) Francl, M. M.; Pietro, W. J.; Hehre, W. J.; Binkley, J. S.; Gordon, M. S.; DeFrees, D. J.; Pople, J. A. *J. Chem. Phys.* **1982**, *77*, 3654. (b) Krishnan, R.; Binkley, J. S.; Seeger, R.; Pople, J. A. *J. Chem. Phys.* **1980**, *72*, 650. (c) Wachters, A. J. H. *J. Chem. Phys.* **1970**, *52*, 1033. (d) Hay, P. J. *J. Chem. Phys.* **1977**, *66*, 4377. (e) Raghavachari, K.; Trucks, G. W. *J. Chem. Phys.* **1989**, *91*, 1062. (f) Binning, R. C.; Curtiss, L. A. *J. Comput. Chem.* **1990**, *11*, 1206. (g) McGrath, M. P.; Radom, L. *J. Chem. Phys.* **1991**, *94*, 511. (h) Clark, T.; Chandrasekhar, J.; Spitznagel, G. W.; Schleyer, P. V. R. *J. Comput. Chem.* **1983**, *4*, 294. (i) Frisch, M. J.; Pople, J. A.; Binkley, J. S. *J. Chem. Phys.* **1984**, *80*, 3265.

(35) Martin, R. L.; Hay, P. J.; Pratt, L. R. *J. Phys. Chem. A* **1998**, *102*, 3565.

(36) (a) Huang, D.; Makhlynets, O. V.; Tan, L. L.; Lee, S. C.; Rybak-Akimova, E. V.; Holm, R. H. *Proc. Natl. Acad. Sci. U. S. A.* **2011**, *108*, 1222. (b) Huang, D.; Makhlynets, O. V.; Tan, L. L.; Lee, S. C.; Rybak-Akimova, E. V.; Holm, R. H. *Inorg. Chem.* **2011**, *50*, 10070.

(37) (a) Liang, Y.; Liu, S.; Xia, Y.; Li, Y.; Yu, Z.-X. *Chem.—Eur. J.* **2008**, *14*, 4361. (b) Chen, Y.; Ye, S.; Jiao, L.; Liang, Y.; Sinha-Mahapatra, D. K.; Herndon, J. W.; Yu, Z.-X. *J. Am. Chem. Soc.* **2007**, *129*, 10773. (c) Yu, Z. X.; Houk, K. N. *J. Am. Chem. Soc.* **2003**, *125*, 13825.

(38) Wen, M.; Huang, F.; Lu, G.; Wang, Z.-X. *Inorg. Chem.* **2013**, *52*, 12098.

(39) Frisch, M. J.; Trucks, G. W.; Schlegel, H. B.; Scuseria, G. E.; Robb, M. A.; Cheeseman, J. R.; Scalmani, G.; Barone, V.; Mennucci, B.; Petersson, G. A.; Nakatsuji, H.; Caricato, M.; Li, X.; Hratchian, H. P.; Izmaylov, A. F.; Bloino, J.; Zheng, G.; Sonnenberg, J. L.; Hada, M.; Ehara, M.; Toyota, K.; Fukuda, R.; Hasegawa, J.; Ishida, M.; Nakajima, T.; Honda, Y.; Kitao, O.; Nakai, H.; Vreven, T.; Montgomery, J. A., Jr.; Peralta, J. E.; Ogliaro, F.; Bearpark, M.; Heyd, J. J.; Brothers, E.; Kudin, K. N.; Staroverov, V. N.; Kobayashi, R.; Normand, J.; Raghavachari, K.; Rendell, A.; Burant, J. C.; Iyengar, S. S.; Tomasi, J.; Cossi, M.; Rega, N.; Millam, N. J.; Klene, M.; Knox, J. E.; Cross, J. B.; Bakken, V.; Adamo, C.; Jaramillo, J.; Gomperts, R.; Stratmann, R. E.; Yazyev, O.; Austin, A. J.; Cammi, R.; Pomelli, C.; Ochterski, J. W.; Martin, R. L.; Morokuma, K.; Zakrzewski, V. G.; Voth, G. A.; Salvador, P.; Dannenberg, J. J.; Dapprich, S.; Daniels, A. D.; Farkas, Ö.; Foresman, J. B.; Ortiz, J. V.; Cioslowski, J.; Fox, D. J. *Gaussian 09*, revision A.01; Gaussian, Inc.: Wallingford, CT, 2009.

(40) (a) Balaraman, E.; Gnanaprakasam, B.; Shimon, L. J. W.; Milstein, D. *J. Am. Chem. Soc.* **2010**, *132*, 16756. (b) Balaraman, E.; Gunanathan, C.; Zhang, J.; Shimon, L. J. W.; Milstein, D. *Nat. Chem.* **2011**, *3*, 609.

(41) (a) Qu, S.; Dang, Y.; Wen, M.; Wang, Z.-X. *Chem.—Eur. J.* **2013**, *19*, 3827. (b) Erdtman, E.; Bushnell, E. A. C.; Gauld, J. W.; Eriksson, L. A. *Comput. Theor. Chem.* **2011**, *963*, 479.

(42) Lim, C.-H.; Holder, A. M.; Musgrave, C. B. *J. Am. Chem. Soc.* **2012**, *135*, 142.

(43) Zimmerman, P. M.; Zhang, Z.; Musgrave, C. B. *Inorg. Chem.* **2010**, *49*, 8724.
(44) (a) Liu, X.-Q.; Jin, L.; Kim, C. K.; Xue, Y. *J. Mol. Catal. A: Chem.* **2012**, *355*, 102. (b) Xue, X.; Yu, A.; Cai, Y.; Cheng, J.-P. *Org. Lett.* **2011**, *13*, 6054. (c) Hall, N. E.; Smith, B. J. *J. Phys. Chem. A* **1998**, *102*, 3985. (d) Hall, N. E.; Smith, B. J. *J. Phys. Chem. A* **1998**, *102*, 4930.
(45) (a) He, L.-P.; Chen, T.; Xue, D.; Eddaoudi, M.; Huang, K.-W. J. *Organomet. Chem* **2012**, *700*, 202. (b) Chen, T.; He, L.; Gong, D.; Yang, L.; Maio, X.; Eppinger, J.; Huang, K.-W. *Tetrahedron Lett.* **2012**, *53*, 4409. (c) He, L.-P.; Chen, T.; Gong, D.; Lai, Z.-P.; Huang, K.-W. *Organometallics* **2012**, *31*, 5208. (d) Zeng, G.; Chen, T.; He, L.-P; Pinnau, I.; Lai, Z.-P.; Huang, K.-W. *Chem.—Eur. J.* **2012**, *18*, 15940.